Recent Progress on Flexible Capacitive Pressure Sensors: From Design and Materials to Applications

Rishabh B. Mishra, Nazek El-Atab, Aftab M. Hussain, and Muhammad M. Hussain*

For decades, the revolution in design and fabrication methodology of flexible capacitive pressure sensors using various inorganic/organic materials has significantly enhanced the field of flexible and wearable electronics with a wide range of applications in aerospace, automobiles, marine environment, robotics, healthcare, and consumer/portable electronics. Mathematical modelling, finite element simulations, and unique fabrication strategies are utilized to fabricate diverse shapes of diaphragms, shells, and cantilevers which function in normal, touch, or double touch modes, operation principles inspired from microelectromechanical systems (MEMS) based capacitive pressure sensing techniques. The capacitive pressure sensing technique detects changes in capacitance due to the deformation/deflection of a pressure sensitive mechanical element that alters the separation gap of the capacitor. Due to advancement in state-of-the-art fabrication technologies, the performance and properties of capacitive pressure sensors are enhanced. In this review paper, recent progress in flexible capacitive pressure sensing techniques in terms of design, materials, and fabrication strategies is reported. The mechanics and fabrication steps of paper-based low-cost MEMS/flexible devices are also broadly reported. Lastly, the applications of flexible capacitive pressure sensors, challenges, and future perspectives are discussed.

1. Introduction

1.1. Pressure as Parameter

Pressure, being one of the most measurable quantities and process parameters, is the ratio of applied normal force over an area with derived measuring unit from three base units of length, mass, and time.[1,2] Several pressure units exist including: pounds per square inch (psi), pounds per square foot (psf), mm Hg, atmospheres (atm), torr, millibar, and pascals (Pa, a.k.a. N m^{-2}). The latter is the most convenient and widely used.

When fluid flows in any pipe section, the pressure is classified as follows:[3]

- Static pressure is due to the stationary fluid (which is not flowing) at the bottom of the pipe (pressure at point X in **Figure 1**a).
- Dynamic pressure is due to fluid flow in which the moving fluid impacts any object or surface (pressure at point Y in Figure 1a).
- Stagnation or impact pressure is total pressure (shown by Y–X in Figure 1a) due to static and dynamic fluid flow where the point at which the stagnation pressure, that is, static pressure, is maximum is called stagnation point.

Instead of pressure measurement of fluid flow in a pipe section, there are three different types of pressure which are measured with respect to vacuum (ideal zero pressure in empty, air-free space) or normal atmospheric pressure (the pressure at earth surface) which can be divided into three different types as follows:

- Absolute pressure (P_0) is measured with respect to vacuum [Figure 1b].
- Gauge pressure (P_{gauge}) is measured with respect to atmospheric pressure [Figure 1b].
- Differential pressure (P_{atm}) is measured with respect to another pressure and is technically the difference of the two pressure values [Figure 1a,c]. If the pressure at the reference point/space is higher than the pressure at the measured point/space, the resultant pressure is known as negative pressure.

1.2. Pressure Sensors: From Conventional, MEMS to Physically Flexible

Several conventional measuring instruments have been used to measure the absolute, gauge, and differential pressure in range of 10^{-7} Pa to hundreds of MPa. McLeod, Knudsen, ionization, Pirani (resistance-thermometer), thermocouples, and viscosity gauges are conventional instruments for measuring

R. B. Mishra, Dr. N. El-Atab, Prof. M. M. Hussain
mmh Labs
Electrical Engineering
Computer Electrical Mathematical Science and Engineering Division
King Abdullah University of Science and Technology (KAUST)
Thuwal 23955-6900, Saudi Arabia
E-mail: mmhussain@berkeley.edu

R. B. Mishra, Dr. A. M. Hussain
Center for VLSI and Embedded System Technology (CVEST)
International Institute of Information Technology (IIIT)
Hyderabad, Telangana 500032, India

Prof. M. M. Hussain
Electrical Engineering and Computer Sciences (EECS)
Cory Hall
University of California
Berkeley, CA 94720-1770, USA

The ORCID identification number(s) for the author(s) of this article can be found under https://doi.org/10.1002/admt.202001023.

ADVANCED
SCIENCE NEWS
www.advancedsciencenews.com

ADVANCED
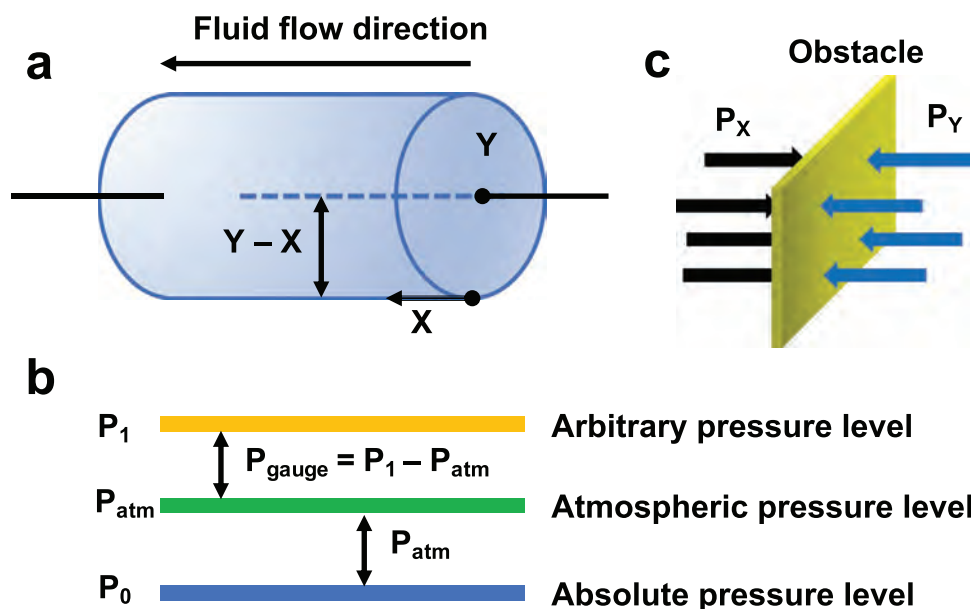**MATERIALS**
TECHNOLOGIES
www.advmattechnol.de

Figure 1. Schematics to define different types of pressure. a) Pipe to show static (X), dynamic (Y), and impact ($Y–X$) pressure. b) Levels to show absolute (P_0), atmospheric (P_{atm}), and differential (P_1) pressure. c) Differential pressure if two different pressures are applied perpendicularly on any obstacle.

vacuum pressure, that is, pressures below atmospheric pressure. For high pressure measurement, greater than atmosphere pressure, conventional devices such as bellows, bourdon tubes, capsules, diaphragms, and strain gauges are utilized for absolute, gauge, and differential pressure measurements, which can reach the MPa pressure range.[1,2,4] Manometers (U-tube, inclined, and wall types) and barometers are the conventional devices used for hydrostatic differential pressure or liquid level measurement. All of these conventional devices are still available for industrial applications and selected according to their suitability, such as pressure measuring range, accuracy, response time, hysteresis, stability, overloading, electrical signal conditioning circuits, or pressure reading requirements.

Advancement of integrated circuit (IC) industry revolutionized MEMS research, specifically after the evolution of surface and bulk micromachining processes.[5] MEMS, the multidisciplinary and one of most popular research areas in CMOS industry, consists of mechanically moveable micro-components such as cantilevers, bridges, diaphragms, valves, gears, channels, and pumps that respond to different physical, chemical, or biological stimuli.[6–11] Pressure microsensors are the most popular devices in the microsensor arena covering a high percentage of the microdevice market.[5,12] The advantages of pressure microsensors over conventional pressure measuring devices are:[5,9,12,13]

- Fast response
- High performance
- Small in size/weight
- Low power consumption
- Large batch fabrication
- Small temperature drift
- High temperature expansion tolerance
- Monolithically integrable with ICs and CMOS circuitry

Due to these significant advantages, the MEMS sensor market is very large despite several challenges including making MEMS devices flexible. However, significant progress has been made toward this purpose, where converting the substrate into its flexible version and using organic and nanomaterials, instead of conventional inorganic semiconductor materials, are found to be the most promising techniques.[14–17] The trend in emerging electronics (i.e., flexible, stretchable, printed, and additive manufactured) is following exponential progress due to the high demand for low-cost, large area, disposable, easily deployable, and skin-like electronic systems that do not compromise performance at any stage/level.[18–20]

In this review paper, we provide a comprehensive report on flexible capacitive pressure sensors in terms of their operation mechanism, type of mechanical sensitive elements, materials used in separation gap between conductive electrodes, and application in different technological sectors, including robotics, wearable/healthcare, aerospace, automobile, biomedical, portable, and consumer electronics, while considering figures of merit.

1.3. Figures of Merit for Pressure Sensing

1.3.1. Static Characteristics

Several parameters are needed to define the performance of capacitive pressure sensors, and which play an important role in understanding the physics of the devices. These parameters include the following:[1,2]

a) Accuracy: The difference between the ideal value (C_{ideal}) versus measured value ($C_{measured}$) of sensor is known as accuracy. This is usually defined in terms of percentage error:

$$\% \in = \frac{C_{\text{measured}} - C_{\text{ideal}}}{C_{\text{measured}}} \times 100 \tag{1}$$

b) Precision: The response of a sensor should be reproducible if the same input is applied multiple times. Therefore, precision describes the reproducibility of sensor and how close the output is from the true value.

c) Resolution: The smallest incremental change in input which produces a detectable change in output (ΔC) is called resolution. This is usually defined in terms of measured range, that is, difference between maximum and minimum input value. If the change in input (ΔP_{min}) can produce the smallest detectable change in output, then maximum resolution is given by:

$$\%R = \frac{\Delta P_{\text{min}}}{P_{\text{max}} - P_{\text{min}}} \times 100 \tag{2}$$

d) Sensitivity: The ratio of incremental output to incremental input is known as sensitivity.

$$S = \frac{\Delta C}{\Delta P} \tag{3}$$

In flexible capacitive pressure sensors, sometimes the normalized form of sensitivity is also used and given by:

$$S = \frac{\Delta C / C}{\Delta P / C} \tag{4}$$

In MEMS, the ratio of deflation in the mechanically sensitive element versus applied pressure is called mechanical sensitivity, while the ratio of change in capacitance and applied pressure range is called electrical/capacitive sensitivity.

e) Non-linearity: The deviation from defined calibration curve (i.e., least square fit or end point straight curve) with experimentally (or simulated) determined output curve is called non-linearity. This is represented as a percentage (%) and is zero for ideal sensors.

$$\%NL = \frac{C_{\text{out}}(P_{\text{ideal}}) - \dfrac{C_{\text{out}}(P_{\text{max}})}{P_{\text{max}}}}{C_{\text{out}}(P_{\text{max}})} \times 100 \tag{5}$$

Here, P_{ideal}, P_{max}, and C_{out} are pressure at calibrated points, maximum operating pressure, and corresponding value of capacitance, respectively.

f) Hysteresis: The maximum difference in output of a sensor at any given measurement point when approaching that point from increasing and then decreasing pressure is known as hysteresis. On a plot of capacitance versus pressure, the loading and unloading curves define this property. Moreover, the value of maximum difference between the area under loading and unloading curves is the hysteresis.

g) Selectivity: If the sensor response is not affected by unwanted signals/noises generated by the environment or other parameters, then the sensor is called selective.

1.3.2. Dynamic Characteristics

Sensors are divided into three categories: First order low-pass, second order low-pass, and bandpass. Partial differential equations relate the quantity under measurement (input) with the sensor output which is analyzed in time and frequency domain for different types of systems. The time and frequency domain analyses are required to define stability, transient response, steady-state response, lead-lag response, damping, response time, rise/fall time, observability, and controllability. In the second order low-pass category, systems are defined as underdamped, overdamped, or critically damped based on the damping factor and location of poles and zeros.[1,2]

1.4. Flexible Capacitive Pressure Sensors

Flexible pressure sensors are one of the most useful devices in the sensors market as compared to other flexible devices. Physical compatibility with any arbitrary curvilinear surface is an important advantage of flexible pressure sensors and has been massively explored for various applications. Pressure measurements can be achieved by designing the devices according to application and transduction principles. Out of the different transduction principles, that is, piezoresistive, capacitive, and piezoelectric, the capacitive transduction technique is the most utilized and explored method due to the following advantages:

- Large fabrication area
- High pressure sensitivity
- Less reactive to temperature drift

1.4.1. Generic Principle of Capacitive Sensing

The capacitive sensing structure consists of two electrically conductive parallel electrodes which are separated by a medium. One of the parallel electrodes is fixed at any curvilinear or non-curvilinear surface while the second electrode is mechanically sensitive. If the overlapping area, separation gap, and permittivity of medium are A, d, and ε, respectively, then the basic capacitance of the structure is given by:

$$C = \frac{\varepsilon A}{d} \tag{6}$$

Note that mathematical Equation (6) does not include fringing field effect.

From Equation (6), it is confirmed that basic capacitance variation can be achieved by altering one or all of the three variables, that is, ε, A, and d, which is employed for pressure sensing. Changing the separation gap is the most utilized technique for capacitive pressure sensing where the separation gap varies as a result of the applied pressure on a mechanical sensitive diaphragm. Parameters like flow rate, permittivity, and displacement are measured/sensed using variations in overlap area (A) and permittivity of the medium (ε).[21–23]

**ADVANCED
SCIENCE NEWS**
www.advancedsciencenews.com

**ADVANCED
MATERIALS
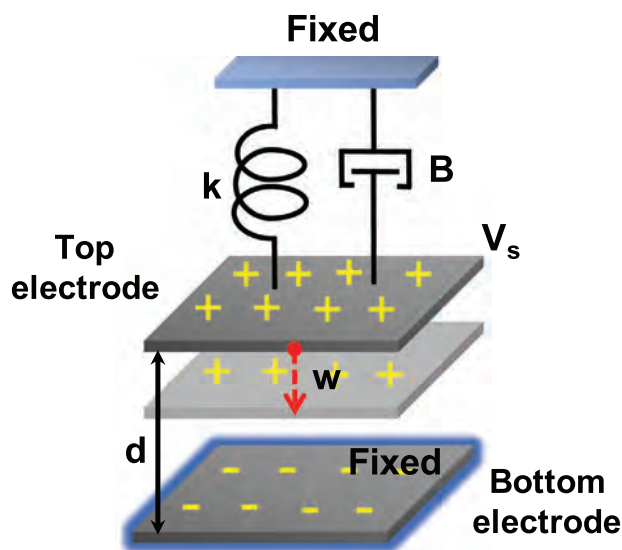TECHNOLOGIES**
www.advmattechnol.de

Figure 2. Schematic of electromechanical model of generic capacitive sensing approach.

1.4.2. Electromechanical Model of Capacitive Sensing

The electromechanical (combination of translational or dynamical) model of parallel plate capacitive pressure sensor [**Figure 2**]. This model consists of a linear spring with spring constant k and damper with damper coefficient B. The mass of the top electrode, overlapping area, initial separation gap, and applied voltage are m, A, d, and V_s, respectively. When pressure is applied on the top electrode, the spring elongates which causes movement of top electrode toward the bottom electrode of the sensor. By choosing proper values of spring constant (k) and damping constant (B) of the spring and damper, respectively, the approximated value of pull-in voltage (V) can be obtained after solving partial differential equation:[24,25]

$$m\frac{d^2w}{dt^2} + B\frac{dw}{dx} + k\,w^2 = \frac{\varepsilon A V^2}{2(d-w)} \qquad (7)$$

where, m and w are mass of moving electrode, deflection in moving electrode.

While performing the normal mode operations, the maximum diaphragm deflection is kept less than one third of separation gap between plate. Different analytical, finite element simulation and lumped model approaches have been tried from different researchers for cantilevers, square, circular, and other shapes diaphragm of capacitive pressure microsensors.[24,25]

2. Electrodes for Flexible Capacitive Pressure Sensors

High performance pressure sensors only require mechanically sensitive diaphragms with conductive electrodes. In fabricating conventional rigid pressure sensors, metallic materials like Au, Ag, Cu, or Al are commonly used as electrode material. Due to technological advancements and reliability enhancement of different fabrication approaches for flexible devices, for example,

printed, additive manufacturing, thermal coating, electrodes made from various low-cost materials can be easily fabricated. The flexible/stretchable electrodes must be conformable, reliable, non-corrosive in humid environment, insoluble, conformable, have large area uniformity and excellent electrical, mechanical, and optical properties, which is becoming more achievable due to advancements in materials science and technologies. The electrode material selection for capacitive pressure sensor is determined by the application of the device, such as implantation,[26] human–machine interface,[27,28] robotics,[29] wearables,[30,31] or electronic skins.[32] In designing flexible electrodes, different next-generation materials like polymers and nanomaterials (normally 1D and 2D) are the most extensively used after indium tin oxide (ITO), thin metallic electrode, and polymeric film. ITO is mechanically rigid in nature and loses its mechanical properties after multiple sensing, bending, and folding operations.[31,33,34] Nanomaterials such as graphene,[34–36] nanotubes,[32,35] nanowires[37,38] are still being explored for designing highly sensitive flexible electrodes for capacitive pressure sensors, however, their basic physical properties such as surface uniformity and conductivity are limited and lack the physical properties of thin film metallic and polymeric electrodes.[39–43] Thus, these nanomaterials are usually sandwiched between two thin films when utilized as electrodes.[32,34–38] B. U. Hwang et al. presented a composite electrode based flexible capacitive pressure sensor in which the top electrode is based on PEDOT:PSS/EMIM-TCB (poly-(3,4-ethylene-dioxy-thiophene):poly-(styrene-sulfonate)/1-ethyl-3-methyl-imidazolium tetracyano-borate), which is piezoresistive in nature while GIG [Au-ITO-AU] is chosen as bottom electrode.[40] The effect of the aspect ratio on cantilever capacitive pressure sensors is analyzed using metal coated polymer as sensing electrode.[39] S. M. Khan et al. analyzed different diaphragm shapes of the same material for acoustic and air pressure sensing[41] and asthma monitoring[42] applications. The top and bottom electrodes are based on graphene while a microstructured polydimethylsiloxane (PDMS) film acts as dielectric in the flexible capacitive pressure sensor.[34] Initially graphene is grown on a copper (Cu) film and then transferred onto a PET (polyethylene terephthalate) sheet. Silver nanowire (AgNW) material has been demonstrated as an electrode in composition with PEDOT:PSS [poly(3,4-ethylenedioxythiophene) polystyrene sulfonate] in a flexible capacitive pressure sensor, in which the AgNWs and PEDOT:PSS are bar-coated on PDMS after patterning. D. J. Lipomi et al. presented an electrode fabricated using carbon nanotubes (CNT) for strain and pressure monitoring using capacitive sensing technique that is flexible, stretchable, and transparent.[32]

3. Types of Flexible Capacitive Pressure Sensors

Capacitive sensing operates by variation of separation gap between plates, overlapping area, or change in dielectric permittivity. Variation in separation gap is the most widely employed pressure sensing approach.[4,43,44] The compression/expansion of the separation gap between parallel plate electrodes changes the capacitance which corresponds to the applied pressure. In this approach, selective design of the dielectric material can

ADVANCED
SCIENCE NEWS
www.advancedsciencenews.com

ADVANCED
MATERIALS
TECHNOLOGIES
www.advmattechnol.de

enhance the sensor sensitivity. In the following, we explore the different dielectric materials used between electrodes in flexible capacitive pressure sensors.

3.1. Air/Vacuum as Dielectric Material

Air/vacuum as the separation gap between electrodes is extensively utilized for most MEMS and flexible capacitive pressure sensors. The dielectric constant of air and vacuum is 1.00059 and 1.0, respectively. Different household materials (e.g., Al-foil, polyimide tape, double sided tape, sponge, microfiber wipe) have been employed in the fabrication of square-shaped flexible capacitive pressure sensors by J. M. Nassar et al.[43] The Al-foil is used as the electrode material which is clamped at the edges using double-sided tape. Three different materials including air, sponge, and microfiber wipe were tested as dielectric material. The sensor in which air acts as the dielectric material showed maximum sensitivity.[43]

When air/vacuum acts as the dielectric material one electrode is highly sensitive to pressure application, which follows the small- or large-deflection theory of plates/shells using continuum mechanics. The small-deflection theory is most widely used to analyze the mechanical performance of MEMS sensors/actuators using mathematical modeling or numerical simulations based on the Kirchhoff–Love plate theory.[45–53] Classical mechanics very efficiently theorizes the parameters of deflection, bending, stress, and strain, as shown by S. P. Timoshenko et al.[8,49,54–56] The analytical investigations for MEMS and flexible capacitive pressure sensors have also been widely explored.[4,39,41,45,46,49,53,55–57] Moreover, the assumptions used to define the mentioned parameters are based on material properties, Hook's Law, and physical properties of plates. The mechanics behind plate deflection has been reported in design of different soft mechanical pressure[58] and force[59] sensors.

The deflection theory has been divided into two parts, that is, small and large deflection theories, based on the diaphragm thickness and has been utilized in a very broad sense for fabricating MEMS and flexible capacitive pressure sensors.[8,39,41,47,50,51,60–63] The small-deflection theory is applicable for thin diaphragms in which deflection is kept less than 1/5th of diaphragm thickness, while large-deflection theory is appropriate for thick diaphragms in which deflection is less than three times its thickness.[50,61,64] Different shapes of diaphragms (i.e., circular, square, rectangular, elliptical, pentagon, hexagon) and modes (normal, touch, double-touch, multi-touch) of capacitive pressure sensors have been reported in this review paper. The goal of the following section is to relate the adoption of microfabrication techniques helpful for the development of polymer and/or paper-based MEMS flexible capacitive pressure sensors.

3.1.1. Cantilever Capacitive Pressure Sensors

A cantilever is basically a mechanical element with one edge fixed/clamped/supported while the other edge is free to move/deflect. This principle has resulted in multiple applications for MEMS and flexible pressure sensors.[39,65–69] Moreover, polymer

and paper cantilevers are being utilized to design low-cost pressure sensors due to advancements in emerging fabrication techniques.[39,70–74] The width to length ratio, that is, aspect ratio, of a capacitive pressure sensor fabricated from metal coated polymer and double-sided post-it tape using do-it-yourself (DIY) emerging fabrication technique, plays an important role for sensing/actuation which has been analyzed for acoustic pressure sensing.[39] As the aspect ratio of sensor decreases the mechanical and electrical sensitivity increases, however the resonance frequency and response time decrease [**Figure 3**a].

3.1.2. Normal Mode Capacitive Pressure Sensors

In microfabrication-based capacitive pressure sensors, the maximum deflection of the diaphragm should be less than 1/3rd of the separation gap between plates to avoid the pull-in phenomenon.[75] Different diaphragm shapes have been reported in design of normal mode capacitive pressure sensors (NMCPS) using conventional microfabrication[75] and also emerging fabrication techniques[41,42] of using paper-like materials such as aluminum (Al) coated polyimide (PI) foil/sheets. In normal mode operation of capacitive pressure sensors, the pressure sensitive diaphragm does not touch the bottom electrode.[62] When the diaphragm shape is changed from square to circular (with sides from 4, 6, 8, and infinity) [Figure 3b] while keeping the overlapping area constant, the diaphragm deflection increases which increases the mechanical and electrical sensitivity of the capacitive pressure sensor,[76] however, the nonlinearity in output response also increases.[41] The sensitivity and non-linearity both again increase when diaphragm shape is modified from rectangular to circular (through the more and less elliptical) shape while keeping overlapping area constant[41] [Figure 3b]. The sensitivity increases as the eccentricity of ellipse tends toward zero, that is, eccentricity of circle. The sensitivity of paper and metal-coated polymer based flexible capacitive pressure sensors with different diaphragm shapes (i.e., circular, square, rectangular, elliptical, pentagon, and hexagon) have been investigated by S. M. Khan et al.[41,42] All of the different shaped sensors have been investigated using acoustic (1 Pa pressure and at different frequencies) testing and air pressure (0–40 Pa pressure range) monitoring. As the diaphragm shape is changed from rectangular toward circular [Figure 3c], both the mechanical and electrical sensitivity increase [Figure 3d,e] however, the linear response of the sensors worsens.[41,42]

3.1.3. Touch Mode Capacitive Pressure Sensors

In MEMS-based touch mode capacitive pressure sensors (TMCPS), the pressure sensitive diaphragm touches the bottom electrode in order to increase the pressure measuring range and the linearity of output response, which could be more robust than NMCPS.[61,77,78] A heterostructure diaphragm (graphene and polymer composite materials) based TMCPS array has been fabricated on thin silicon substrate, however, any other material could be utilized in place of silicon, as the researchers proposed for future work.[79,80] Commercially available household materials, like Al-coated polyimide (PI) foil and
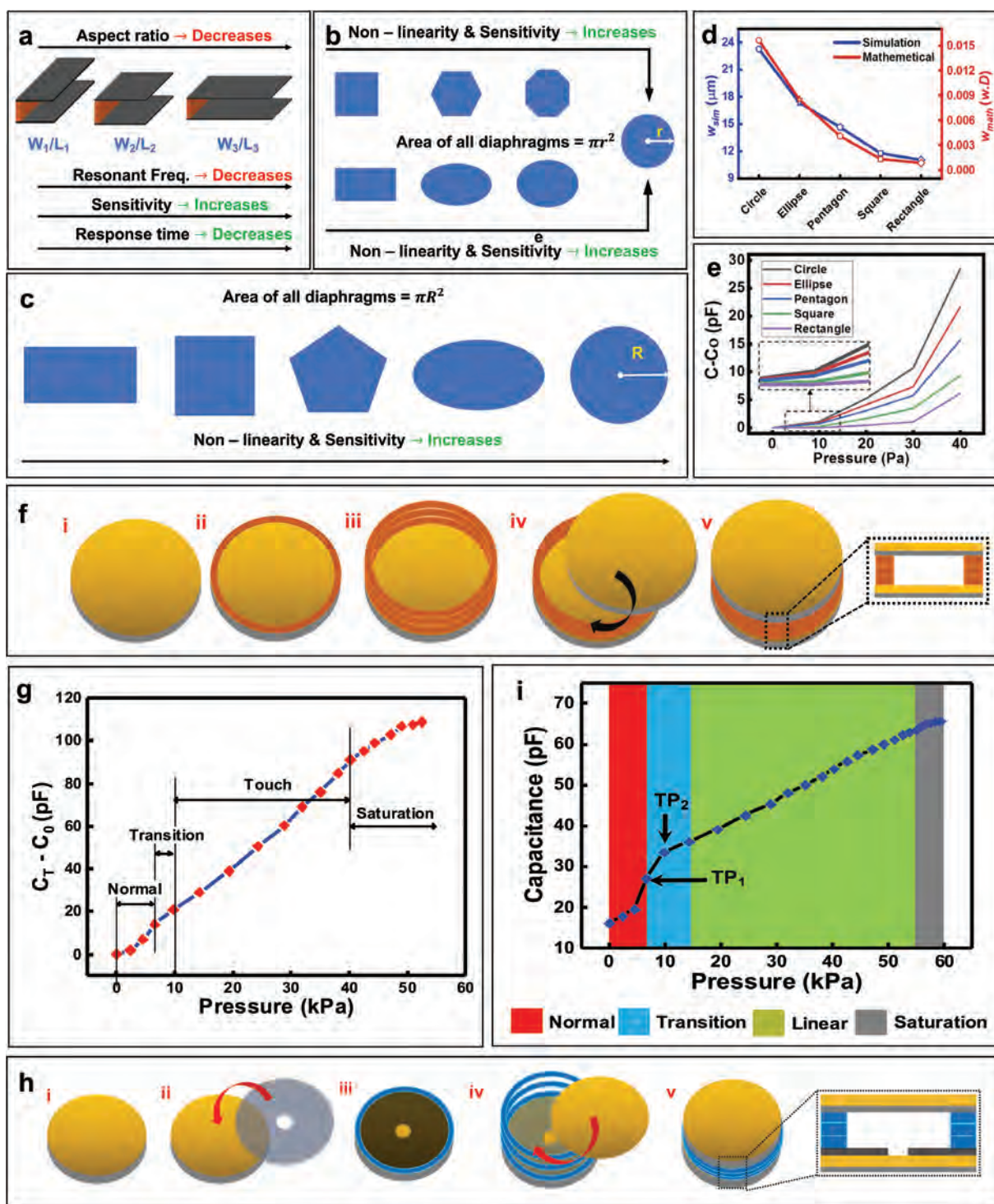
Figure 3. Flexible capacitive pressure sensor with air dielectric and different operation modes of normal, touch, and double touch to study effect of shape and size of mechanical sensing element. a) Effect of cantilever aspect ratio on the performance parameters sensitivity, response time, and resonant frequency. b) Effect on nonlinearity and sensitivity when the diaphragm shape changes from square to circle (with sides from 4, 6, 8, and ∞) and rectangle to circle (through the elliptical shape) while keeping overlapping area same. The sensitivity increases as the eccentricity of ellipse tends toward zero, that is, from more elliptical to less elliptical and then circular shape of diaphragm. c) Effect on nonlinearity and sensitivity of five different diaphragm shapes (rectangle, square, pentagon, ellipse, and circle) in paper-based capacitive pressure sensor. d) Investigation (mathematical and finite element simulations) of deflection in different diaphragm shapes after 1 Pa pressure application. e) Variation of change in capacitance versus applied pressure on different shapes of paper-based NMCPS. (d,e)—Reproduced with permission.[4] Copyright 2020, AIP. f) Fabrication process flow of designing TMCPS. g) Experimental characterization of TMCPS to show different operating regions. (f,g)—Reproduced with permission.[81] Copyright 2020, IEEE. h) Fabrication process flow of designing DTMCPS. i) Experimental characterization of TMCPS to show different operating regions.

**ADVANCED
SCIENCE NEWS**
www.advancedsciencenews.com

**ADVANCED
MATERIALS
TECHNOLOGIES**
www.advmattechnol.de

double-sided tape, are utilized for designing flexible TMCPS.[81] The sensor is fabricated [Figure 3f] by cutting two circular pieces from Al-coated PI sheet and then using three layers of double-sided tape along the edges to paste the pieces together. The sensor is characterized using an air pressure set-up and Figure 3g shows the different regions of operation, that is, normal (0–8 kPa), transition (8–10 kPa), linear (10–40 kPa), and saturation (after 40 kPa) regions.[81]

3.1.4. Double and Multi Touch Mode Capacitive Pressure Sensors

The double touch mode capacitive pressure sensor (DTMCPS) is introduced to increase pressure measurement and linear operation range.[82,83] MEMS-based DTMCPS have been previously theoretically explained[82,83] (mathematical and finite element simulations) and fabricated[82] by different researchers. H. Lv et al. optimized the physical parameters (dimensions and diaphragm thicknesses) for fabricating DTMCPS as compared with TMCPS.[82] Al-coated PI sheet, PI tape, and double-sided tape is again utilized to design the DTMCPS where the fabrication steps are shown step-by-step in Figure 3h.[84] The PI tape with small circular hole is placed on top of circular piece and then three layers of double-sided tape are placed at the edges

of PI tape, which provides support to the diaphragm that is placed on top of the double-sided tape layers. The different operation regions of DTMCPS, normal (0–7.5 kPa), transition (7.5–14.24 kPa), linear (14.24–54.9 kPa), and saturation (above 54.9 kPa) [Figure 3i].[84]

3.2. Graphene and Graphene Oxide as Dielectric

Graphene and graphene-polymer composite materials have been extensively used for designing electrodes for capacitive pressure sensors, however, some researchers have presented flexible capacitive pressure sensors using graphene-polymer composites and graphene-based materials as the dielectric.[85–89] H. Ze et al. presented graphene and porous-nylon network as dielectric material for flexible capacitive pressure sensors.[86] **Figure 4**a shows the fabrication process flow in which PDMS provides mechanical support to the graphene while the silver strip acts as the electrode. The combination (sandwiched layer) of graphene and porous-nylon netting with different micro-sized meshes (150, 75, 35 μm) and different thicknesses (55, 48, 34 μm) acts as dielectric material. After pressure application, the separation gap between the PDMS layers decreases and a change in capacitance occurs. The experimental
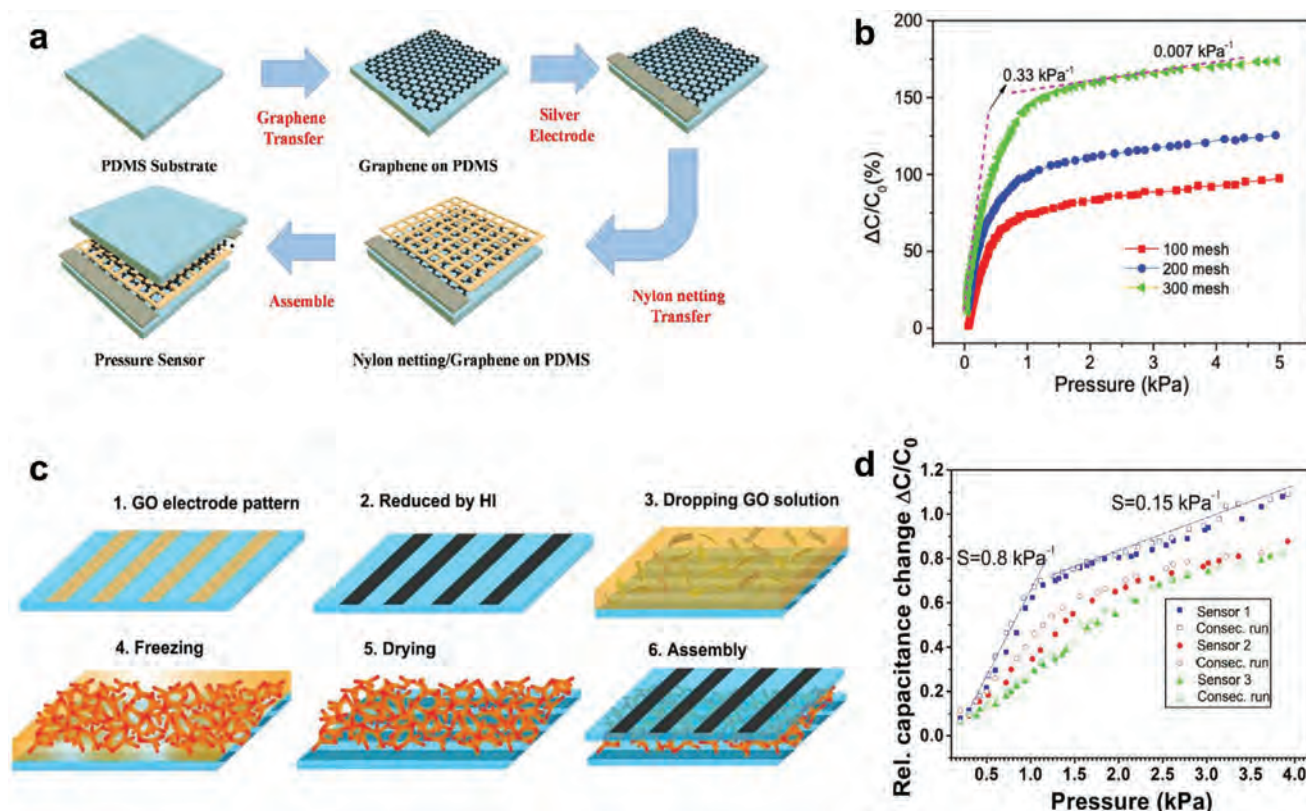

Figure 4. Example of graphene and graphene-based dielectric materials for flexible capacitive pressure sensors. a) Fabrication steps for flexible capacitive pressure sensor using graphene and porous nylon network as dielectric. b) Sensor response with three different meshes of porous nylon network. (a,b)—Reproduced with permission.[86] Copyright 2018, ACS. c) Fabrication steps of graphene oxide (GO) dielectric material based flexible capacitive pressure sensors. d) Sensor response shows the change in capacitance with pressure variation. (c,d)—Reproduced with permission.[88] Copyright 2017, Elsevier.

**ADVANCED
SCIENCE NEWS**

www.advancedsciencenews.com

**ADVANCED
MATERIALS
TECHNOLOGIES**

www.advmattechnol.de

characterization [Figure 4b] shows sensor operating range up to 5 kPa with sensitivity of 0.33 kPa^{-1} and 0.007 kPa^{-1} for 0–1 kPa and 1–5 kPa^{-1}, respectively, and with response time of <20 ms.

S. Wan et al. fabricated a pressure sensor in which they used graphene oxide (GO) as the dielectric material.[88] Figure 4c shows the fabrication steps in which GO is printed on PET sheet and then reduced by hydrochloric acid (HI). In the next step, the GO is dropped onto the GO printed sheet and placed inside a microwave oven chamber for freezing and drying, then, another reduced GO printed PET sheet is placed on top of the dry GO which acts as the pressure sensitive top electrode. The sensor response is measured for 0–4 kPa pressure range with response time of ≈100 ms and sensitivity of 0.8 and 0.5 kPa^{-1} for 0–1 kPa and 1–4 kPa, respectively [Figure 4d].

For high pressure measurement, two composites, branched-carbon nanotubes (b-CNTs) and graphene nanoplatelets (GNP), are mixed in different proportions with thermoplastic polyurethane (TPU) and utilized as dielectric material.[89] The flexible capacitive pressure sensor of b-CNTs and GNP composite material in 3:1 ratio shows the best sensitivity among all other compositions, which is 2.05 MPa^{-1} for 0–1.2 MPa pressure range.

3.3. Porous Elastomers/Foam/Sponge/Composites as Dielectric

Different types of elastomers like Ecoflex and PDMS have played important roles in the design of flexible capacitive pressure sensors. Other materials that have been composited with these elastomers to make porous, sponge-like, and foam-like material are highly flexible even after curing at normal room temperature. These porous and sponge like dielectric materials consist of air/bubble gaps which make them highly compressible and able to regain their original thickness after the pressure is released. A low-cost flexible capacitive pressure sensory array has been demonstrated which has highly flexible polymeric foam as dielectric.[90] The flexible foam-based pressure sensor is characterized by placing four different weights on the sensor [**Figure 5**a]. The foam-based sensory skin, which has 90 pressure sensing elements, has been demonstrated in the application of object detection on the shelf of a retail store [Figure 5b]. The foam-based PDMS/Ecoflex used as dielectrics and is spray-coated AgNWs as electrode on two parallel side of dielectrics to design the flexible capacitive structure.[28] The PDMS/Ecoflex foam is prepared at 80 and 120 °C temperatures from 33% concentration by weight [Figure 5c]. The sensors are characterized at different temperatures for various curing temperatures and concentrations of PDMS/Ecoflex. As an application demonstration, the pressure sensor is placed on human chest for respiration monitoring. The same foam is utilized to design a pressure 8 × 8 sensory skin/matrix [Figure 5d] which is also characterized using different weights [Figure 5e].

During the last few years, fabric-based electronics have shown progress in design of flexible and hybrid electric devices.[91,92] A silicone elastomer material and conductive fabric (knitted and woven) based soft and flexible capacitive pressure sensor is designed by O. Atalay et al.[92] The conductive fabrics act as parallel plate electrodes and 3D printed silicone material as dielectric, [Figure 5f]. When pressure is

applied on the conductive electrodes, the silicone elastomer collapses which results in a change in capacitance corresponding to pressure application. To analyze the primary change in capacitance, two types of unstructured fabrics, knit and woven, are used. The sensor with knit electrodes gave better sensitivity (2.3 MPa^{-1}) than the woven electrodes (0.7 MPa^{-1}), however, the response of the knit electrode-based sensor is more non-linear than the woven electrode based sensor, while the knit fabrics are bulkier and consist of more non-smooth surfaces as compared to the woven fabrics [Figure 5g]. Yet, for achieving higher sensitivity the knit fabric is more suitable for any kind of application. To improve sensitivity, the electrodes are micro-structured, and the dielectrics are filled with sugar and salt to create micro-porosity. The sensitivity of the sensor with sugar dielectrics and micro-structured electrodes is 12.1 MPa^{-1}, while the sensor with salt dielectric and micro-structured electrode has sensitivity of 4.5 MPa^{-1} [Figure 5h].

To enhance sensitivity of flexible capacitive pressure sensors, sponge-based dielectric materials have also been widely explored. A PDMS/graphene sponge-like dielectric sandwiched between Cu electrodes is presented in the design of a wireless flexible capacitive pressure sensor (Figure 5i–k).[87] The sponge consists of graphene and the existing air holes form multiple parallel capacitors which compress during pressure application. The multiple parallel capacitors provide an overall large change in capacitance. The sponge-based dielectric pressure sensor showed higher sensitivity (0.12, 0.042, and 0.004 kPa^{-1} for 1–10, 10–100, and 100–500 kPa pressure range, respectively) than a sensor using normal PDMS dielectric [Figure 5l]. A porous PDMS has been composited with yeast and sandwiched between ITO/PET electrodes to enhance sensitivity by C. Parameswaran et al.[93] The fabricated sensor robustness does not change even after multiple testing, which can be seen by the topographical image in Figure 5m. The sensor sensitivity decreases as the thickness and weight of PDMS is increased with maximum sensitivity of 0.55618 kPa^{-1} for 0.5 gm of PDMS [Figure 5n].

3.4. Wrinkled Dielectrics

To enhance the sensitivity of flexible pressure sensors wrinkled structures have been extensively utilized in both resistive[94–97] and capacitive[98–102] pressure sensing techniques. The fabrication mechanism is basically stretching and then releasing the dielectric material. After releasing, wrinkles are generated as the dielectric material resumes its original state. Silver nanowires (AgNW) embedded PDMS with wrinkled structures are one of most utilized materials for flexible capacitive pressure sensor fabrication. Y. Joo et al. developed a multiscale structure based robust flexible capacitive pressure sensor using wrinkled PDMS.[99] The fabrication begins with UV/O$_3$ treatment of stretched PDMS followed by bar-coating of AgNWs on the stretched PDMS. The liquid PDMS is poured on the AgNWs and cured at 65 °C for 12 h in air. The cured PDMS is peeled-off and then placed on poly(methyl methacrylate) [PMMA] or poly(4-vinylphenol) [PVP] which acts as the dielectric and has an inkjet-printed Ag electrode (**Figure 6**a). The sensor is
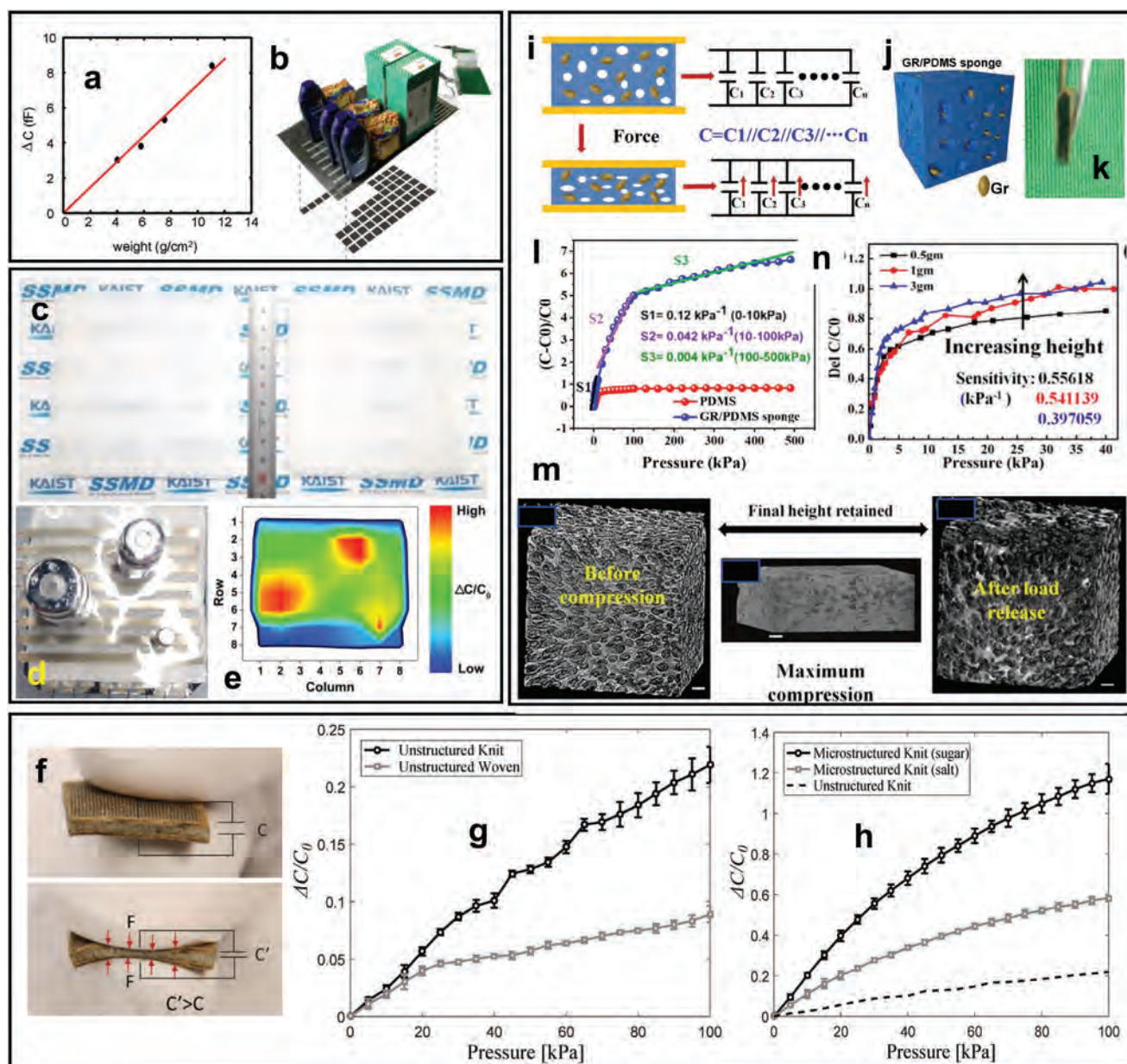
Figure 5. Examples of porous elastomers/foam/sponge/composites like dielectrics-based flexible capacitive pressure sensors. a) The response of single pressure sensor w.r.t. applied load. b) Sensory matrix of 90 pressure sensors for object detection on grocery store shelf. (a,b)—Reproduced with permission.[90] Copyright 2008, AIP. c) Photograph of fabricated PDMS/Ecoflex dielectric material for flexible capacitive pressure sensor at 80 and 120 °C. d) Photograph of placing 10, 100, and 200 g weights on 8 × 8 pressure sensory skin. e) Response of pressure sensory skin which corresponds to applied pressure from different weights. (c–e)—Reproduced with permission.[28] Copyright 2020, RSC. f) Photograph of actual fabricated flexible capacitive pressure sensor in normal condition and when pressure is applied. g) Response of pressure sensor for two different unstructured textile electrodes, that is, unstructured knit and woven. h) Response of pressure sensor when the woven and knit electrodes are micro-structured and silicone dielectrics have salt and sugar microporous materials as compared with unstructured knit electrode. (f–h)—Reproduced with permission.[92] Copyright 2017, Wiley. i) Schematic to show pressure sensing from PDMS/graphene sponge dielectric sandwiched between Cu electrodes in flexible capacitive pressure sensor. j) Schematic to show configuration of PDMS/graphene sponge under pressure application. k) Photograph of wireless pressure sensor to show the flexibility. l) Response of pressure sensor to show sensitivity as compared to normal PDMS dielectric layer of same thickness and overlapping area between plates. (i–l)—Reproduced with permission.[87] Copyright 2019, Nature Research. m) Topographical image of PDMS/yeast composited sponge at normal, maximum compressed, and released state. n) Response of flexible capacitive pressure sensor to reveal sensitivity under different weights and thicknesses of PDMS/yeast composited dielectric layer. (m,n)—Reproduced with permission.[93] Copyright 2018, RSC.

characterized for 0–4.5 kPa pressure range with sensitivities of ≈3.8 kPa⁻¹, ≈0.8 kPa⁻¹, and ≈0.35 kPa⁻¹ for 0–0.5 kPa, 0.5–2.5 kPa, and 2.5–4.5 kPa⁻¹, respectively (Figure 6b).

Fabricated 3 × 3 and 5 × 5 sensory matrices show same sensitivity as a single sensor for object detection and spatial distribution of pressure.
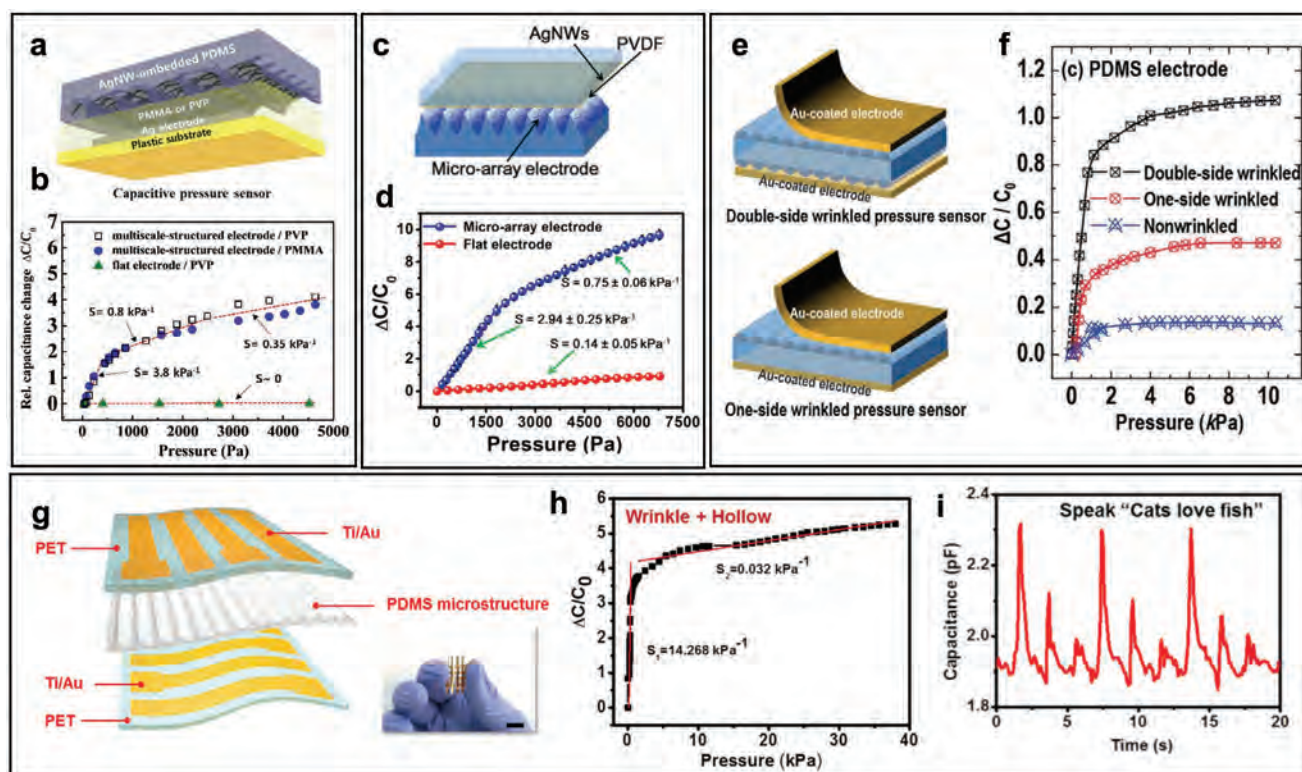
ADVANCED
SCIENCE NEWS
www.advancedsciencenews.com

ADVANCED
MATERIALS
TECHNOLOGIES
www.advmattechnol.de

Figure 6. Examples of wrinkled dielectric based flexible capacitive pressure sensors. a,b) Schematics of wrinkled AgNW embedded PDMS based flexible capacitive pressure sensor with PMMA or PVP as dielectric layer and the pressure sensor response to determine sensitivity. Reproduced with permission.[99] Copyright 2015, RSC. c,d) Schematics of AgNW electrode with wrinkled PDMS and the pressure sensor response compared with an unstructured dielectric based pressure sensor. Reproduced with permission.[37] Copyright 2017, ACS. e,f) Schematics of one and double sided wrinkled Ecoflex templet with Au-coated PDMS electrode and sensor response comparison of double sided and one sided wrinkled Ecoflex with non-wrinkled dielectrics. Reproduced with permission.[98] Copyright 2017, RSC. g) Schematics of wrinkled PDMS dielectric based flexible capacitive pressure sensor with Ti/Au electrodes on PET substrate that provides mechanical support. The inset photograph shows sensor flexibility with scale bar of 1 cm. h) Response of pressure sensor of hollow and wrinkled PDMS for 0–40 kPa pressure range. i) Response of sensor demonstrated to detect vocal cord vibration of subject pronouncing "cats love fish." (g–i)—Reproduced with permission.[100] Copyright 2019, ACS.
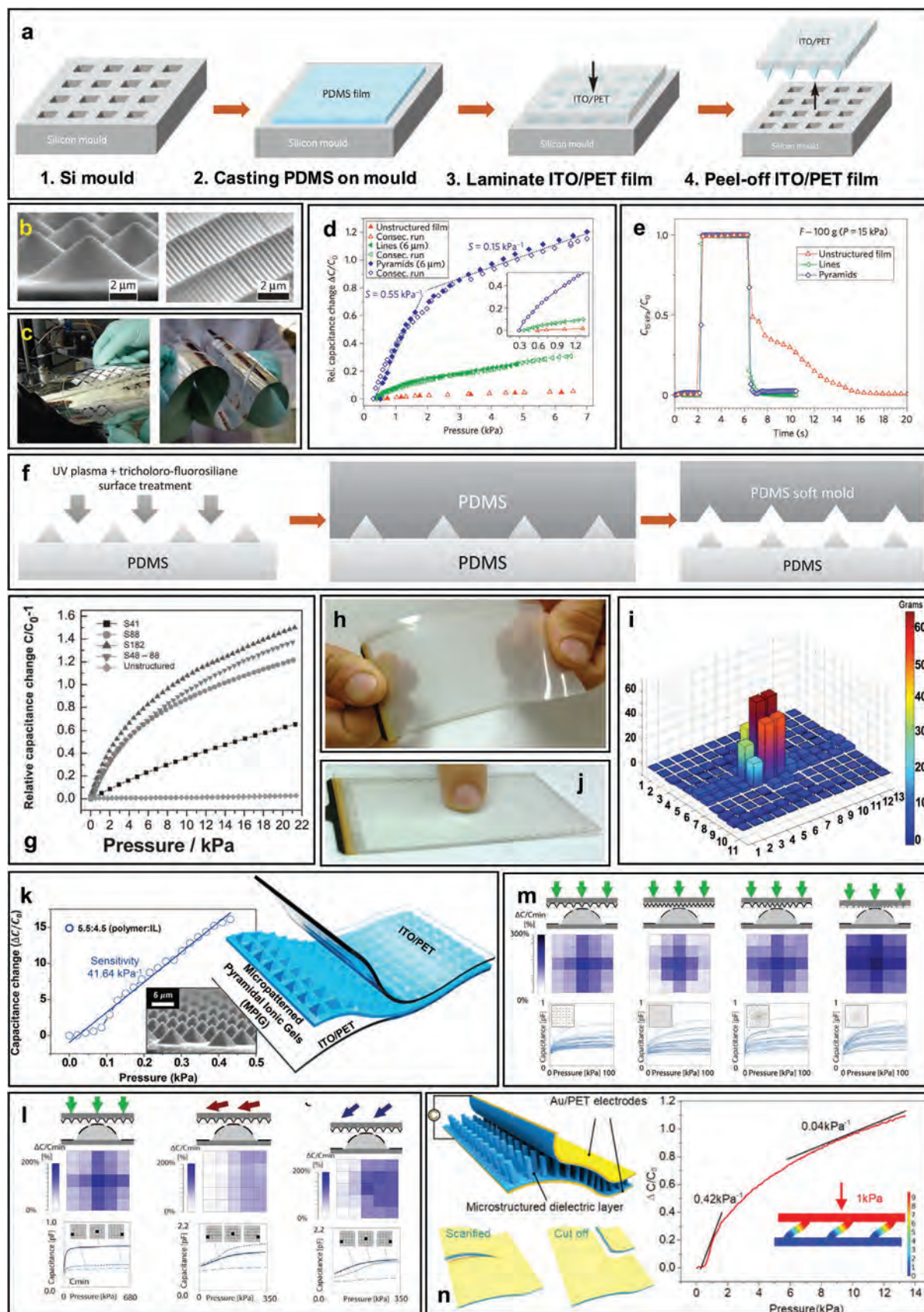
Prof. C.-P. Wong's group fabricated AgNWs embedded wrinkled PDMS based flexible capacitive pressure sensors for demonstration of wearable and healthcare applications.[37,101] The sensor consists of two layers of PDMS, one is wrinkled with AgNWs electrode while the other is normal PDMS with embedded AgNWs (Figure 6c). The sensor fabricated by X. Shuai et al. exhibited a sensitivity of 2.94 ± 0.25 and 0.75 ± 0.06 kPa^{-1} for 0–2 and 2–9 kPa, respectively, for a minimum detection limit of less than 3 Pa (Figure 6d).[37]

Double-sided wrinkled-based low-cost flexible capacitive pressure sensor (Figure 6e) for large-area sensing using Ecoflex as soft material placed between two Au coated PDMS electrodes has been reported by S. Beak et al.[98] The double-sided wrinkled-based sensor has lower response time (578 ms, 782 ms), recovery time (0.0012 kPa^{-1} for <1 kPa) and sensitivity (4.2 × 10^{-6} kPa^{-1} for 1–10 kPa) than one-sided and non-wrinkled pressure sensors (Figure 6f). Hollow-wrinkled structures on PDMS are being utilized as dielectric materials to enhance the sensitivity of PDMS wrinkled based flexible capacitive pressure sensor, as reported by X. Zeng et al.[100] The structured dielectric material is sandwiched between Ti/Au patterned PET substrate which provides mechanical stability to the flexible capacitive pressure sensor and also acts as electrode (Figure 6g). The sensor

is characterized for 0–40 kPa pressure range with sensitivity of 14.268 and 0.032 kPa^{-1} for 0–0.7 and 0.7–40 kPa pressure ranges (Figure 6h) and response time of less than 50 ms. Due to the enhanced sensitivities, ultra-low response and recovery time, the sensor has enough potential to monitor human physiologies. Vocal recognition is presented as an example application by demonstrating sensor response (Figure 6i) when a subject speaks "cats love fish."

3.5. Micro-Structured Elastomers as Dielectric

Micro-pillars, micro-bumps, and micro-structures as dielectric material have been widely explored for more than a decade in the design of highly sensitive flexible capacitive pressure sensors.[103,104] Micro-arrays are developed by casting PDMS on silicon mold and then ITO/PET thin film that acts as electrodes is laminated on the PDMS [**Figure 7**a].[105] After peeling off the ITO/PET thin film from the silicon mold, the PDMS micro-arrays are formed, as shown in the scanning electron microscope (SEM) image [Figure 7b]. The pressure sensors fabricated using the presented technique are mounted at full wafer scale on any kind of flexible or plastic substrate with high uniformity

**ADVANCED
SCIENCE NEWS**

www.advancedsciencenews.com

**ADVANCED
MATERIALS
TECHNOLOGIES**

www.advmattechnol.de

**ADVANCED
SCIENCE NEWS**
www.advancedsciencenews.com

**ADVANCED
MATERIALS
TECHNOLOGIES**
www.advmattechnol.de

[Figure 7c]. The characterization results show the capacitance versus pressure plot for 0–7 kPa pressure range with 0.55 and 0.15 kPa^{-1} sensitivities at 0–2 kPa and 2–7 kPa, respectively [Figure 7d]. The rise and fall time, or relaxation time, after pressure application of 15 kPa [Figure 7e]. The fall time for the pressure sensor with unstructured PDMS dielectric is very high (almost 10 s), however, the response time or rise time of pressure sensors with structured and unstructured PDMS materials are almost identical in millisecond range.

B. C. K. Tee et al. (from Prof. Z. Bao's group at Stanford University) simulated stress on different micro-pillars with various sidewall angles (54.7°, 65.8°, 76°, and 90°) and found that as the sidewall angle decreases the strain on the micro-pillar also decreases.[106] Moreover, the separation gap between the micro-pillars was also simulated and found that as the separation gap between micro-pillars increases the strain also increases. The fabrication of PDMS micro-pillars [Figure 7f] starts with KOH-etching of <100> silicon wafer. PDMS soft molds are utilized to achieve micro-pillars and placed on rigid silicon substrate to provide mechanical stability to pillars for characterization. The authors fabricated micro-pillars with different separation gaps, 41, 88, 182, and 41–88 µm, represented as S41, S88, 182 µm, and S48–S88. Out of these separation gaps, the S41 sample had maximum sensitivity while the unstructured sensor sample had minimum sensitivity [Figure 7g]. A sensor "skin" matrix is fabricated using 130 sensor pixels with flexibility [Figure 7h] and the matrix response [Figure 7i] when the pressure is applied from a fingertip [Figure 7j].

M. Lee et al. designed a micro-structured dielectric based flexible capacitive pressure sensor in which one electrode is deposited on the microstructure while the other electrode is a layer of Parylene/ITO/PET.[107] PDMS is spin-coated on a mold of KOH-etched <100> silicon pyramidal microgrooves. After peeling-off the PDMS, which then has micro-pillars, Ti/Au is deposited on the micro-pyramids. The other electrode is based on a combination of Parylene/ITO/PET which is fabricated in two steps, laser etching of ITO followed by Parylene deposition. Moreover, both the electrodes, that is, Ti/Au-deposited PDMS micro-structures and Parylene/ITO/PET, are aligned and bonded. The authors presented mathematical explanations of capacitance variation in this orientation of electrodes and experimentally characterized the sensory skin, which has a sensitivity of 70.6 and 3.3 kPa^{-1} for 0–50 Pa and >50 Pa, respectively. V. Palaniappan et al. grooved square patterns on an acrylic sheet using CO_2 laser to create a mold for which PDMS solution is poured on top of.[108] Two samples are prepared and oriented on top of each other so that the tips of the micro-structures face each other. The sensor was characterized for 0–10 kPa pressure range with 2.21, 0.33, and 0.11 kPa^{-1} sensitivities for pressure range of 0–100 Pa, 100–1000 Pa, and 1–10 kPa, respectively. The reported response time, recovery time, and hysteresis of sensor is 50 ms, 150 ms, and 0.7% for more than 1000 experimental cycles.

S. H. Cho et al. patterned micro-pillars using ionic gels with height of 5 µm and area of 5 × 5 µm^2,[109] as the inset SEM image shows in Figure 7k. The micro-pillars are sandwiched between ITO/PET thin sheets which act as parallel plate electrodes [Figure 7k]. The sensory skin has sensitivity of 41.64 and 13 kPa^{-1} for <400 Pa pressure and 0.5–5 kPa pressure range, respectively. This sensory electronic skin has excellent response time (<20 ms), small rise and fall time and low operating voltage (0.25 V), however, the challenge of this pillar arrangement is to sense shear force, bending and lateral strain. To overcome this challenge, C. M. Boutry et al. designed hierarchical micro-patterns in which the dielectric has both micro-bumps and micro-pillars sensitive to not only normal, but also shear pressure, combination of shear and normal pressures, as well as bending conditions.[110] The response of electronic skin, that is, capacitance variation with pressure, was measured for all three cases of pressure application. The electronic skin sensor consists of an array of capacitors with top electrode fabricated using CNTs and polyurethane (PU), [Figure 7l]. The bottom layer has

---

Figure 7. Examples of micro-structured dielectrics based flexible capacitive pressure sensors. a) Different steps to show fabrication of micro-structures using Si mold. The fabricated PDMS micro-pillars are sandwiched between ITO/PET and acts as flexible capacitive pressure sensory skin. b) SEM images of micro-structured PDMS. Left: 2D-arrays of square micro-pyramids. Right: Uniformity and regularity in micro-structures after fabrication. c) Photograph of PDMS micro-structures mounted on flexible plastic substrate to show flexibility. d) Relative capacitance variation w.r.t. applied pressure to show the sensitivity of micro-structured PDMS dielectric based flexible capacitive pressure sensory skin as compared with unstructured PDMS dielectrics. The inset shows response of sensor at low pressure application. e) Relative capacitance variation due to 15 kPa pressure application for 4 s to show the response time for micro-structured and unstructured PDMS dielectrics. The fall time of micro-structured PDMS dielectrics is in milliseconds unlike 10 s for unstructured PDMS dielectrics. (a–e)—Reproduced with permission.[105] Copyright 2010, Nature Research. f) Steps to fabricate PDMS micro-pillars using PDMS soft molds. g) Relative capacitance variation w.r.t. applied pressure for different separation gaps of micro-structured PDMS, S41, S88, and S182 corresponds to separation gap of 41, 88, and 182 µm, respectively. Here, S48–88 is the sample with 48 and 88 µm pillars. h) Photograph to show the flexibility of sensory skin consisting of 130 pressure sensors. i,j) Response of sensory skin consisting of 130 pressure sensors when pressure is applied by fingertip. (f–j)—Reproduced with permission.[106] Copyright 2014, Wiley. k) Flexible capacitive pressure sensors with micro-pillars of ionic gels. The SEM image of micro-pillars are shown in the inset and sensitivity of pressure sensory skin is 41.64 kPa^{-1} for 0–0.5 kPa pressure range. Reproduced with permission.[109] Copyright 2017, ACS. l) Experimental characterization of 5 × 5 pressure sensory skin, which is centered on single micro-bumps, with normal, shear, and combination pressures. Capacitance variation plots for the three kinds of pressure are also shown. m) Response of fabricated 5 × 5 capacitive pressure sensory e-skin with orthogonal and spiral pyramids. Top: cross-sectional view with normal/perpendicular force (green). Middle: sensitivity magnitude for the all 25 sensors in e-skin. Bottom: response curves for all 25 capacitors. Left two figures: 30 µm wide pyramids positioned along orthogonal grid for two different ratios of b/a, 4 and 0.4, respectively. Third figure from left: 10 µm wide pyramids positioned along phyllotaxis spiral grid for two different ratios of b/a, 0.4 and 4. Rightmost figure: 10 mm wide pyramids positioned along phyllotaxis spiral grid for ratio of b/a, 0.4 and 4. (l,m)—Reproduced with permission.[110] Copyright 2018, AAAS. n) Tilted micro-pillars as dielectric material for flexible capacitive pressure sensor with Au/PET as electrodes and sensory skin sensitivity of 0.42 and 0.04 kPa^{-1} for low (0–2 Pa) and high (2–14 Pa) pressure range, respectively. The tilted micro-pillar has better sensitivity than unstructured and vertical micro-pillars of PDMS determined using finite element simulations with deflections at 1 kPa shown in the inset. Reproduced with permission.[111] Copyright 2017, ACS.

**ADVANCED
SCIENCE NEWS**

www.advancedsciencenews.com

**ADVANCED
MATERIALS
TECHNOLOGIES**

www.advmattechnol.de

micro-bumps (diameter = 1 mm and height = 200 μm) and top layer has micro-pyramids (electrode width = 300 μm, and separation gap between two consecutive micro-pyramids = 50 μm) placed on each other facing orthogonally. The 5 × 5 sensory skin is designed with various separation gaps between micro-pillars [Figure 7m]. Characterization shows that as the ratio of separation gap between micro-pillars to width of micro-pillars (*b*/*a*) increases, the sensitivity of the electronic skin increases. In Figure 7m, the top row shows the position and separation gap of micro-pillars, the middle row shows the pressure sensed by the electronic skin array and the bottom row is the normalized capacitance to show sensitivity. Y. Luo et al. designed tilted micro-pillars as dielectric to enhance sensor sensitivity, specifically targeting high sensitivities in low pressure range for application in wearable and smart robotics [Figure 7n].[111] The steps for fabricating these micro-pillars are quite similar to others but with a 30° tilt which, as confirmed by finite element simulations, deflect more resulting in higher sensitivity than bulk and vertical oriented dielectric materials [Figure 7n]. The sensor with tilted micro-pillars has sensitivities of 0.42 and 0.04 kPa^{-1} for 0–2 and 2–14 kPa pressure ranges [Figure 7n].

3.6. Fluidic/Ionic Liquids as Dielectric

Sensitivity has been one of the critical parameters in pressure sensors and employing micro-structures as dielectrics has significantly contributed to improving it. Nevertheless, sensitivity is still limited by the pressure measurement range due to low compressibility which reduces the reliability of sensors/electronic skins after multiple loading and unloading cycles.[112] To overcome this challenge, ionic fluids and Iontronics have been reported by several research groups. Iontronics is a very new, emerging and interdisciplinary research area which combines electronics with ionics employing physical, chemical, biological sciences, and engineering.[113] Ionic liquids offer multiple advantages such as improved flexibility, signal intensity, and sensitivity of sensors simply because ions provide electric double layer (EDL) capacitance.[114] N. Bai et al. presented a graded intra-fillable architecture (GIA) based iontronic flexible pressure sensor [**Figure 8**a].[112] The fabrication steps [Figure 8b] begins with the GIA-based PVA/H$_3$PO$_4$ film (blue) being casted and cured on sandpaper. The sandpaper has holes which generate undercuts and grooves in the casted and cured PVA/H$_3$PO$_4$ film. After peeling off from sandpaper, is the film is sandwiched between Au (yellow) electrode and PI (violet) which provides mechanical support to the structures. The sensor is characterized for 0–360 kPa pressure range [Figure 8c] which has sensitivities S1, S2, and S3 of 3.3, 0.67, and 0.23 Pa^{-1} for 0–10, 10–100, and 100–360 kPa, respectively. Q. Liu et al. designed a highly transparent (transmittance of 90.4%) flexible capacitive pressure sensor using ionic liquid as dielectric layer.[114] The ionic liquid is poured into a porous polyvinylidene fluoride (PVDF) film which has identical refractive index and increasing the transmittance of PVDF film from 0% to 94.8% in the visible spectrum. The ionic liquid filled PVDF film is sandwiched between two Ag nanowire (AgNW) electrodes which are transparent with 97.6% transmittance [Figure 8d]. The sensor is characterized for 0–120 kPa pressure range with 1.194 and

0.109 kPa^{-1} sensitivities for 0–0.5 and 0.5–120 kPa, respectively [Figure 8e].

Prof. T. Pan's group at University of California Davis extensively explored ionic liquid and iontronic-based flexible capacitive pressure sensors. B. Nie et al. presented micro-droplet (electrolyte/glycerol) based circular shaped flexible capacitive pressure sensor [Figure 8f] with broad analysis toward device optimization for blood-pressure sensing applications.[115] The EDL capacitor is made using micro-droplets as dielectric medium located between ITO electrodes mechanically supported by PET substrate. The authors have considered multiple radii (1.5, 3, 6, and 9 mm) of sensing element with multiple heights of sensing chamber (0.14, 0.21, 0.28, and 0.35 μm) and various volumes of micro-droplets (0.3, 0.6, 2, and 3.6 μL) [Figure 8g–j]. After characterizing the devices, the optimum one (radius = 9 mm, micro-droplet volume = 3 μL, height of sensing chamber = 140 mm, and sensitivity = 1.58 μF kPa^{-1}) is placed at carotid artery for real time continuous monitoring of blood pressure. Following this work, B. Nie et al. presented iontronic-based 12 × 12 flexible capacitive pressure sensor array with high sensitivity (0.43 nF kPa^{-1}) over large pressure range which is suitable for surface topology mapping and wrist pulse monitoring.[116] The interfacial circumference area between the EDL capacitor parallel plates and dielectric fluids expands after pressure application [Figure 8k]. For fabricating the pressure sensors, four kinds of imidazolium-based ionic liquids are used with three different pixel sizes (1, 2, and 3 mm with pressure sensitive element thickness = 75 μm) and three different pressure sensitive membrane thicknesses (75, 125, and 175 μm with pixel size = 2 μm). The characterization results for six different samples [Figure 8l,m] and clearly indicates that spatial resolution and thickness of pressure sensitive membrane strongly affects the performance of the sensor array. As the pixel size increases from 1 to 3 mm, the sensitivity of sensor also increases from 3.9–433.7 pF kPa^{-1}, however, the sensitivity decreases from 77.7 to 7.8 pF kPa^{-1} as the thickness of pressure sensitive element increases from 75 to 175 μm. Z. Zhu et al. designed epidermal flexible capacitive pressure sensors where ionic fluid is utilized as dielectric material that is 85% optically transparent.[117] The authors introduced epidermal–iontronic interface (EII) based capacitive pressure sensor [Figure 8n]. The ionic electrode is mechanically sensitive deforming under pressure application and makes epidermal ionic contact with human skin. As the applied pressure increases, the contact area between electrodes, that is, epidermal ionic contact, increases which produces a relative change in capacitance w.r.t. applied pressure. The sensors are square shaped and fabricated with various combinations of pressure sensitive membrane lengths, membrane thicknesses, and adhesive thicknesses. Different pressure sensitive membrane lengths (2, 4, and 6 mm) are investigated while keeping membrane thickness (75 μm) and adhesive thickness (50 μm) constant, then different sensing membrane thicknesses (75, 125, and 175 μm) while keeping sensing length (6 mm) and adhesive thickness (50 μm) constant, and finally, varied adhesive thicknesses (50, 100, 150, and 200 μm) while keeping sensing area and membrane thickness (75 μm) constant. Characterization results are shown in Figure 8o–r and the sensor with membrane length of 6 mm, membrane thickness of 75 μm and adhesive thickness of 50 μm which had sensitivity of
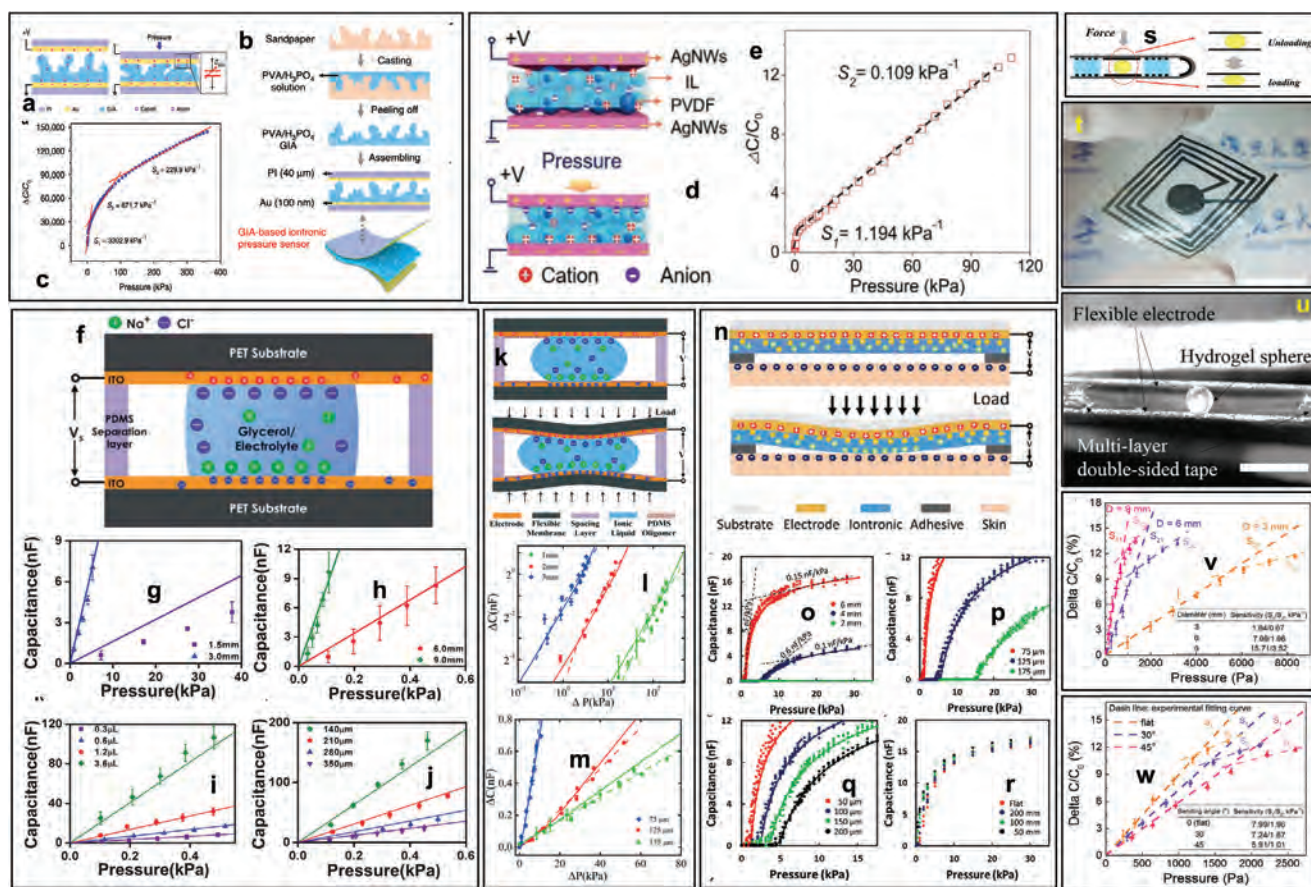
Figure 8. Examples of fluidic/ionic liquid dielectric based flexible capacitive pressure sensors. a) Schematics of pressure sensor with GIA dielectric material. b) Step-by-step fabrication process of GIA-based flexible capacitive pressure sensors. c) Response of GIA-based flexible capacitive pressure sensors. (a–c)—Reproduced with permission.[112] Copyright 2020, Nature Research. d) Schematic showing sensing principle of sensor composed of ionic liquid with PVDF sandwiched between parallel electrodes. e) Response used to define sensor sensitivity. (d,e)—Reproduced with permission.[114] Copyright 2020, Wiley. f) Schematic to show sensing principle of droplet (glycerol/electrolyte)-based interfacial capacitive pressure sensor. g,h). Sensor response for four different radii of sensing chambers, that is, 1.5, 3, 6, and 9 mm. i) Sensor response for four different volumes of droplets, that is, 0.3, 0.6, 1.2, and 3.6 mL. j) Sensor response for four different heights of sensing chambers, that is, 140, 210, 280, and 350 mm. (f–j)—Reproduced with permission.[115] Copyright 2012, RSC. k) Schematic of interfacial capacitive sensing principle using ionic liquids. l) Response of pressure sensory skin with three different spatial resolutions whose pixel sizes are 1, 2, and 3 mm for sensing membrane thickness of 75 μm. m) Response of pressure sensory skin with three different sensing membrane thicknesses of 75, 125, and 175 μm for pixel size of 2 mm. (k–m)—Reproduced with permission.[116] Copyright 2014, RSC. n) Schematic of EII-based flexible capacitive pressure sensor with iontronic dielectric layer. o) Response of pressure sensor for three different lengths of sensing area, that is, 2, 4, and 6 mm, with sensing membrane thickness and adhesive thickness of 75 and 50 μm, respectively. p) Response of pressure sensor for three different sensing membrane thicknesses, that is, 75, 125, and 175 μm, with length of sensing area and adhesive thickness of 6 mm and 50 μm, respectively. q) Response of pressure sensor for four different adhesive thicknesses, that is, 50, 100, 150, and 200 μm, with length of sensing area and sensing membrane thickness of 6 mm and 75 μm, respectively. r) Response of pressure sensor on flat and three different surface curvatures, that is, 50, 100, 200 mm. (n–r)—Reproduced with permission.[117] Copyright 2017, Wiley. s) Photograph of fabricated wireless flexible capacitive pressure sensor. t) SEM image of fabricated capacitive pressure sensor showing the cross-section and contact position of IAH microsphere. u) Response of sensor for three different diameters of sensing area, that is, 3, 6, and 9 mm. v) Response of sensor for three different bending angles, that is, flat, 30° and 45°. The inset tables show sensitivity of different conditions. (s–v)—Reproduced with permission.[118] Copyright 2017, Wiley.

5 and 0.15 nF kPa^{-1} in 0–5 and 10–30 kPa pressure ranges was the optimized sensor. This sensor is suitable for wearable applications that focus on blood pressure, respiration rate, muscle activity, and tactile sensation monitoring.

A challenge for the ionic liquid based capacitive pressure senor is to transmit data wirelessly by keeping the device dimensions optimal. Y. Tai et al. presented a chip-like wireless flexible capacitive pressure sensor in which ionic alginate hydrogel (IAH) micro-sphere was used as the dielectric material.[118] In first step, conductive micro-patterns are printed on PET substrate and double-sided tape is placed on one side of

the patterned PET substrate. In second step, 0.2 μL volume of hydrogel sphere is placed in the patterned PET substrate and then the PET substrate is folded and assembled [Figure 8s,t]. In response to pressure application, the micro-sphere deforms, covering more area of the overlapping plate and, simultaneously, the separation gap between parallel plates decreases producing a corresponding change in capacitance. For device optimization, pressure sensors with different sensing diameters, that is, 3, 6, and 9 mm, are experimentally characterized resulting in sensitivities of 1.84, 7.99, and 15.71 kPa^{-1}, respectively [Figure 8u]. The sensor with 6 mm diameter was characterized

ADVANCED
SCIENCE NEWS

www.advancedsciencenews.com

ADVANCED
MATERIALS
TECHNOLOGIES

www.advmattechnol.de

under different bending angles [Figure 8v] showing that as the bending angle increases (from 0 to 45 degrees), the sensitivity of sensor decreases (from 7.99 to 5.91 kPa^{-1}).

3.7. Fibers as Dielectrics

The conductive fibers and textiles are becoming popular day by day for designing various sensors, actuators, energy harvesting devices which are obtaining great attention which significantly contributed for sensitivity enhancement of flexible capacitive pressure sensor with cost effective approach with only few easy processes which is utilized for flexible and wearable electronics a lot in past few years.[119–123] The conductive fiber-based textile based capacitive pressure sensor[120] is presented for wearables from Prof. T. Lee group at Yonsei University, which is one of the major contributions toward sensitivity enhancement of flexible capacitive pressure sensors. The fabrication of sensor matrix starts with the preparation of conductive Kevlar fiber (which is strong synthetic fiber and heat resistant) which is coated with poly(styrene-block-butadienstyrene) (SBS) polymer and AgNP. Thereafter, PDMS is coated on the AgNP/SBS composite electrode to provide mechanical stability and protect the electrodes. The conductive fibers are then stacked first to fabricate 2 × 2 sensory matrix and characterized. The sensory matrix shows pressure sensitivity of 0.21 and 0.064 kPa^{-1} for less than 2 kPa and more than 2 kPa, respectively with negligible hysteresis. The conductive functional fibers are stacked and incorporated with wearable gloves to wireless controlling of the drone and hexapod robot. Almost same fabrication mechanism is being utilized with Twaron fibers with solid and microporous PDMS coated on the AgNP/SBS composite.[119] The conductive fabric coated with microporous PDMS shows sensitivity of 0.278, 0.104, and 0.0186 kPa^{-1} for less than 2, 2–10, and 15–50 kPa, respectively with 6.3% hysteresis, about 340 ms response time and 38.82 Pa of lowest detection limit.

3.8. Printed Dielectrics

The printing technique has also been used in the development of sensitivity and cost-effective flexible capacitive pressure sensors in last few years. B. B. Narakathu et al. demonstrated the fabrication of a fully printed flexible capacitive pressure sensor using both conventional screen and gravure printing techniques.[124] The sensor was based on a flexible PET substrate with a metallization layer based on silver nanoparticles ink, while PDMS was employed as the dielectric layer. The silver nanoparticles were deposited using the gravure printing technique while the PDMS dielectric layer was screen printed. In fact, gravure printing is a robust process which enables high printing speeds with high quality in addition to allowing the use of low viscosity inks. The screen printing technique shares the same advantages with the addition of allowing the deposition of a generally larger wet film thickness as opposed to other printing methods. The main fabrication parameters that affect the quality of the screen printed films include pressure on the stencil, squeegee height, speed, snap-off, and offset for the screen stage, which all need to be optimized depending on the material being printed and the substrate being used. The sensor was able to detect a minimum pressure of 800 kPa where the capacitance changed from 26 to 28 pF, while the maximum detectable pressure was 18 MPa which led to a 40% change in the measured capacitance. Moreover, the authors reported a stable performance of the sensor where the recorded variability in the capacitance between various devices was in the 0.15% range. Similar materials were used by A. Eshkeiti et al. from the same group, for the fabrication of a flexible capacitive pressure sensor,[125] however, in this case, both the dielectric material, based on PDMS, and the metallization layer based on silver ink, were screen printed on a PET substrate. It should be noted that in these works, the response time and sensitivity at the highest operating pressure were not reported. The minimum and maximum detectable pressures were 0.2 and 2.4 MPa, respectively, leading to capacitance changes of 1% and 3.6%, respectively.

In another work, S. Khan et al. developed a flexible capacitive pressure sensor by sandwiching two screen printed layers with good alignment.[126] The first stack included adding electrodes based on silver paste on a PI substrate followed by the screen printed of a piezoelectric material polyvinylidene fluoride-trifluoroethylene P(VDF-TrFE) with a thickness of 3 μm. The second stack included silver paste based electrodes on a PET substrate. Next, both stacks were sandwiched together with good alignment resulting in a flexible pressure sensor with a sensitive area of 1 mm^2. However, the authors did not study the capacitance change at different applied pressures, instead the piezoelectric response of the sensor was recorded which is not within the scope of this review paper. CNTs-based screen printed electrodes have also been reported in the development of flexible pressure sensors. D. Maddipatla et al. used a 1.15 mm thick PDMS layer as the dielectric material in combination with screen printed CNTs electrodes.[127] The sensor was capable of detecting various pressures ranging from 15 up to 337 kPa where an 8.2% change in capacitance was recorded, leading to a sensitivity of 0.021% change in capacitance per kPa. Nevertheless, the response time and active area of the sensors were not reported. Z. Guo et al. also reported a pressure sensor based on CNTs, however, in this case the CNTs were mixed with PDMS and used as the dielectric layer, while silver ink was screen printed to form the electrodes.[128] The demonstrated sensor showed a maximum sensitivity of 2.9 kPa^{-1} when operated over a pressure range of 0–450 Pa. To achieve this, the optimization of the concentration of the CNTs in the DMS electrodes was necessary. The authors reported that an aspect ratio of CNTs of 1250–3750 with a weight fraction of 3.75%, in addition to a pyramidal shape of PDMS/CNTs were compulsory to achieve the highest sensitivity, where the relative permittivity of the composite dielectric layer is increased under pressure. Several arrays of the sensors were also developed by the authors showing an excellent uniformity and spatial resolution. Nevertheless, the response time of the sensors was also not reported.

The 3D printing technique has also been demonstrated for the development of flexible capacitive pressure sensors. In fact, the 3D printing technique has received a growing interest due to its low cost and simplicity, in addition to the availability of flexible filaments for both dielectric and conductive materials. To this end, M. Schouten et al. reported a flexible pressure

ADVANCED
SCIENCE NEWS
www.advancedsciencenews.com

ADVANCED
MATERIALS
TECHNOLOGIES
www.advmattechnol.de

senor that was fully printed and based on parallel plates.[129] The printed materials include conductive and insulator based thermoplastic TPU. The devices with an active area of 3×3 mm^2 were tested under a pressure range of 33–55 kPa where a 160 fF change in capacitance was recorded at the maximum operating pressure. This low sensitivity has been explained by the authors as being due to the stiffness of the 3D printed electrodes, the sensitivity can also be enhanced by printing the dielectric using a lower infill percentage. Nevertheless, it should be noted that the pressure range for maximum sensitivity was not studied in this work. Inkjet printing has also been employed in the fabrication of flexible pressure sensors, which enables low cost, resourceful materials usage with a high speed and patterning capability. M. Kisić et al. printed silver nanoparticles ink on two PI-based membranes.[130] In fact, PI membranes were used as the dielectric layer and spacer of the sensor, thus, when pressure is applied, the membranes would deflect and cause the reduction in the spacing between the electrodes and leading to an increase in the measured capacitance. The authors reported a sensitivity of 16.7 pF per bar at pressures ranging from 0 up to 1 bar (100 kPa), however, an extensive characterization of the sensors is missing.

4. Discussion on Various Design Approaches with Advantages and Challenges

In this review article, our approach is to characterize the flexible capacitive pressure sensors based on the dielectric materials and designs which have been extensively utilized recently. We started first to explain the sensors with air as the dielectric material, then, with graphene/graphene oxide, micro-structured and then fluidic dielectrics while considering that the sensitivity enhancement approach should be followed by all of them.

J. M. Nassar et al.[43] designed the paper based flexible capacitive pressure sensor with microfiber wipe, sponge, and air. Among all of these three materials, the pressure sensor with air dielectric shows maximum sensitivity because the air is highly compressible than the remaining two which enabled design of the paper-watch for health monitoring.[30] In spite of this advantageous property—the air is easily available in environment, nevertheless, the flexible pressure sensors always should show excellent mechanical durability which increases the repeatability, and therefore, the sensor could sustain large amounts of pressure without degradation in its performance after multiple testing. The sensors with air dielectric gap always require mechanical support whenever the large area of diaphragm is chosen for designing large area sensor modules[131] otherwise the mechanically sensitive diaphragm is deflected at the center due to the prestress and gravity effect.[81,132] The major issue with air dielectric is that whenever the air particles squeeze after pressure application, damping is caused which degrades the performance of the sensors.

To overcome the challenges of the air dielectric based flexible capacitive pressure sensor, graphene, and graphene oxides and some porous materials including different porous elastomers,[28,90,93] sponge,[43,87] microfiber wipe,[43] nano-mesh,[131] have been utilized as dielectrics. These porous materials

include some amount of air either in bubble form or air molecules which are present between the threads or wires. The advantages of porous materials are basically: enhanced mechanical stability, mature and well-developed fabrication technique of the porous materials using elastomers, and high surface to volume ratio. In order to enhance the performance of the sensor, the design approach has been well studied including the use of wrinkled and micro-structures which are discussed in sections 3.4 and 3.5 of this review. The wrinkled dielectrics are generally fabricated from the elastomers which are stressed first and then sandwiched between two electrodes and next released. In the terms of sensitivity and other parameters enhancement, the wrinkled dielectrics approach is quite better than using porous materials, however controlling the wrinkles[133,134] and fast output saturations are major challenges which have been reported previously. Therefore, to overcome the challenges that the wrinkled dielectric approach faces, micro-structuring of the dielectric material has been previously explored to enhance the sensitivity of the sensors, in addition to enabling a fast response time and allowing the design of pressure sensors for both high- and low-pressure monitoring. Prof. Z. Bao group from Stanford University showed the first demonstration of flexible capacitive pressure sensors using the shape and size optimization, pillar orientations, and combination of micro-pillers and micro-bumps technique.[104,105,110,135]

With the recent advancement in ionic gels and liquids in addition to the iontronic technique, the ionic fluidic dielectrics have received an increased attention and were explored extensively for sensitivity and flexibility enhancement, rather than focusing on the micro-structuring approach. The flexible capacitive pressure sensors with fluidic dielectrics are highly sensitive for small pressure ranges, very compatible with wearables, in-vivo and in-vitro measurements.[136] Moreover, using fluidic dielectrics in combination with a proper electrode material enable the design of transparent[114] flexible capacitive pressure sensors as opposed to the various structures and designs of dielectrics which have been reported and classified before. The major challenges which are being reported for fluidic dielectric based flexible pressure sensors are fluid leakage issues and integrating the iontronic devices with biocompatible integrated circuitries which could be lead to an excellent technological achievement in neuro-prosthetics and artificial cardiac pacemakers.[136]

The fibers/fabrics and printing approaches are also explored a lot which contribute a major part for designing the flexible capacitive pressure sensors. Utilizing these materials reduces cost of the device because of easy availability, well developed fabrication steps/approaches, and does not require the cleanroom environment for fabrications. In fact, the printing technology overcomes several of the challenges that are faced by the traditional silicon technology which requires high vacuum, deposition of films at high temperatures in addition to expensive lithography tools. The main advantages of the screen printing approach include a reduced waste of material during the development, enhanced cost efficiency, reduced operation and manufacturing temperatures, in addition to the possibility of using various types of substrates with flexing capabilities. Nevertheless, to achieve a low cost and high performance system, different electronic components need to be fabricated using a printing-based or a compatible fabrication technique,

ADVANCED
SCIENCE NEWS
www.advancedsciencenews.com

ADVANCED
MATERIALS
TECHNOLOGIES
www.advmattechnol.de

moreover, scaling down the pressure sensors could be limited when using a printing technique when compared with the conventional silicon technology.

5. Applications of Flexible Capacitive Pressure Sensor

5.1. Aerospace Applications

The aerospace industry requires very precise and wide range pressure monitoring for different purposes such as altitude monitoring, weather forecasting, air speed and wind pressure monitoring, payload transfer for military application[48,137–140] in unmanned aerial vehicles (UAVs), orbital satellites, space aircrafts, and other aerospace vehicles. L. Lin et al. presented a MEMS piezoresistive pressure sensor using surface micromachining process with 2 μm thick square shaped diaphragm for 100 Psi ($\approx$689.5 kPa) full scale pressure monitoring.[48] X. Lü et al. presented a low cost flexible capacitive pressure microsensor made of PDMS dielectric material and copper electrodes with polyethylene terephthalate (PET) utilized for encapsulation.[137] A common challenge is the sensor placement on the curvilinear surfaces of aerodynamic systems. W. Xiong et al. addressed this challenge for futuristic smart UAVs [**Figure 9**a] in their skin-like flexible capacitive pressure sensor array designed using PDMS, polyimide (PI) and epoxy, and experimentally characterize for 3 kPa full scale pressure range. The skin-like sensor array, which includes four units of pressure sensors, is placed on a hollow cylinder [Figure 9b] to demonstrate flexibility.[138] Aerodynamic systems require placement of flexible pressure sensor skin on aircraft wings [Figure 9a,c] for wind pressure monitoring.[138,141,142] The flexible capacitive pressure sensor skin presented for air speed detection consists of one reference unit and five sensors [Figure 9d,e] connected through a miniaturized pipe [Figure 9d] to transfer air from the inlet at the reference sensor.[141,142] The different pressure values, that is, P_1, P_2, P_3, P_4, and P_5, are then subtracted from P_0 which is the pressure output from the reference sensor. These measured values are used to calculate a single readout vector employed to obtain the value of dynamic air pressure or wind pressure.[141,142] H. Shi et al. designed a skin-like soft and flexible capacitive pressure sensor matrix for measuring positive and negative pressure in –60 to 20 kPa range.[143] The sensor matrix is designed using low cost polymer materials PEDOT:PSS and Ecoflex, encapsulated with PDMS (schematic in Figure 9f and 12 × 12 sensor array matrix in Figure 9g).[143]

5.2. Automotive Applications

A significant amount of progress has been made for MEMS-based capacitive pressure sensors for the automobile sector,[144–147] however, new and emerging technologies based on flexible pressure/strain sensors are on-trend for various types of monitoring, such as tire pressure, gas exhaust, airbag, vehicle detection, and in-vehicle monitoring of driver and passengers for long travel.[147–152] C. K. Duc et al. designed flexible capacitive pressure sensors using Al foil as electrode material and

polyurethane film as dielectric material [Figure 9h], for wireless vehicle detection.[151] The sensor is experimentally characterized at different high pressures of 1.5 MPa full scale value [Figure 9i] and mounted on the road (without reconstruction) [Figure 9j] to estimate the speed and weight of vehicles with an error rate of 10.83% and 0.33% at the maximum values of speed and weight, respectively.[151] S. Cruz et al. designed a fully inkjet-printed flexible capacitive pressure sensory matrix (inset of Figure 9k) for posture imbalance monitoring, which could be helpful for the driver and other passengers when travelling long distances.[150] The presented sensor shows high linearity [Figure 9k] up to almost 50 kPa pressure range with reported sensitivity of 40–50 pF Pa^{-1}.[150]

5.3. Marine Applications

Pressure sensing in ocean and marine environments has been a major research challenge over the last few decades due to the harsh conditions and is still being explored today.[11,153–158] M. M. Hussain's group at King Abdullah University of Science and Technology (KAUST) presented standalone, lightweight, low-cost CMOS compatible, and multisensory marine skin for deep sea environment monitoring.[155,156] This multisensory marine skin [Figure 9l] monitors marine environment, that is, pressure, depth, temperature, and salinity, when tagged onto diverse animals, for example a deep sea crab (*Portunus pelagicus*) (Figure 9m).[155] The fabricated flexible capacitive pressure sensor is circular with Ti/Au chosen as top/bottom electrode and PDMS as the dielectric material. The PDMS thickness is optimized according to full scale pressure, flexibility, stretchability, and signal saturation in output, which is characterized in 10–11 dbar pressure range [Figure 9n] at 21 °C and 0, 3.62, and 2.54 cm bending radiuses.[155] The pressure increases linearly with sensitivity of 6.93 pF cm^{-1} and 0.71 nF per dbar [Figure 9n] as the animal descends in sea depth.[155]

5.4. Robotics Applications

Sensors and artificial skin for robotics have primary application in tactile perception where touch sensing is a very promising and revolutionized area of research. Several significant approaches in this interdisciplinary research area will be discussed. Robotic e-skin plays an important role for well-organized and controlled monitoring to fulfill the desired requirements of the most promising applications in automation and medical industries. This begins with placement of flexible and stretchable systems/devices on the robotic hand for monitoring of various parameters.[159–161]

5.4.1. Flexible Capacitive Pressure Sensors for Robotic Grippers

L. Chin et al. presented a soft robotic gripper [**Figure 10**a] consisting of highly sensitive flexible capacitive pressure and strain sensor used for object sorting, capable of distinguishing material with puncture resistance.[162,163] This soft robotic gripper
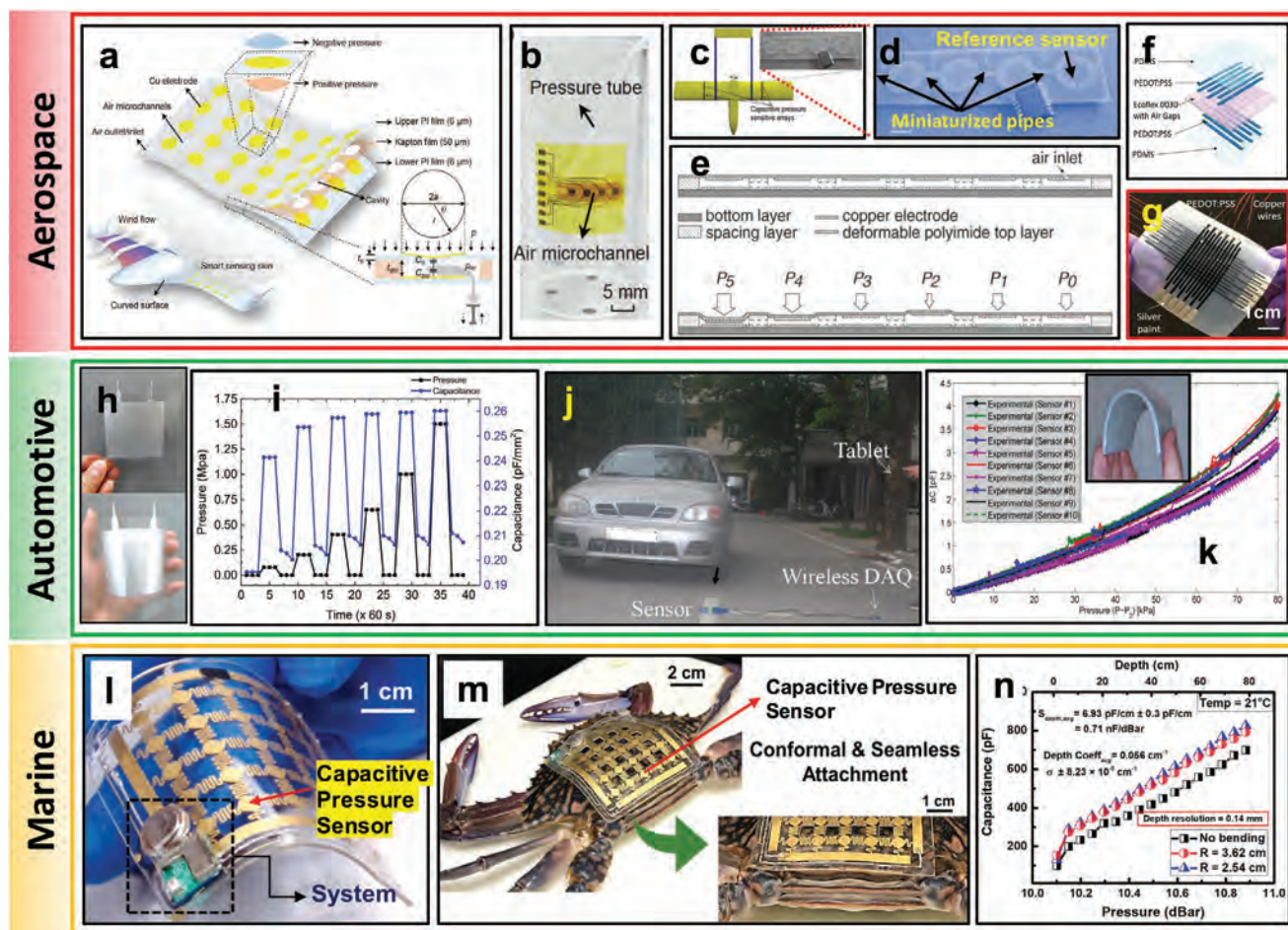
**ADVANCED
SCIENCE NEWS**

www.advancedsciencenews.com

**ADVANCED
MATERIALS
TECHNOLOGIES**

www.advmattechnol.de

Figure 9. Flexible capacitive pressure sensor for aerospace, automotive and marine applications. a) Schematic of aircraft equipped with pressure sensory skin in which the sensor has circular shaped capacitive pressure sensing element of radius = a. b) Fabricated flexible capacitive pressure sensor array (4×1) mounted on a hollow cylinder. (a,b)—Reproduced with permission.[138] Copyright 2020, Springer. c) Schematic of sensory skin placement on wings of UAV and inset SEM image of the sensors. Reproduced with permission.[141] Copyright 2006, Elsevier. d) Colored SEM image of capacitive pressure sensors on printed circuit board strip (PCB) showing the reference sensor connected to all other sensors through a miniaturized pipe. Reproduced with permission.[142] Copyright 2005, Elsevier. e) Schematic of capacitive pressure sensor array where the sensor measuring P_0 pressure has a small air inlet hole. Reproduced with permission.[141] Copyright 2006, Elsevier. f,g) Schematic of flexible and soft capacitive pressure sensor fabricated using PEDOT:PSS and Ecoflex with PDMS utilized for encapsulation and fabricated flexible capacitive pressure sensor matrix of 12×12. Reproduced with permission.[143] Copyright 2019, Wiley. h) Flexible capacitive pressure sensor fabricated using Al foil as electrode material and polyurethane film. i) Experimental characterization of sensor for 1.5 MPa full scale pressure. j) Sensor mounted on road for wireless monitoring of vehicle speed and weight. (i,j)—Reproduced with permission.[151] Copyright 2019, MDPI. k) Response of fully inkjet-printed flexible capacitive pressure sensor for monitoring posture imbalance. Reproduced with permission.[150] Copyright 2015, IEEE. l) Marine skin demonstrating the flexibility of sensor system which consists of flexible capacitive pressure, temperature, and salinity sensor fabricated using low-cost CMOS compatible approach and encapsulated using PDMS. m) Marine skin attached onto crab (*Portunus pelagicus*) to monitor its movement in the sea. n) Output of marine skin capacitive pressure sensor to monitor underwater depth by measuring increased pressure. (l–n)—Reproduced with permission.[155] Copyright 2018. Nature Research.

is capable of grasping objects with 1–10³ MPa compliance and of 20–25 mm radius.[162] The same robotic gripper is capable of sorting recycled materials of paper, plastic, and metal due to placement of flexible capacitive pressure and strain sensor on its one finger.[163] J. Hashizume et al. reported a robotic grasper of comparatively compact size which can grasp any object with high pull-out force on rough surface using soft-rubber based large-area soft and flexible capacitive pressure sensor on adhesive film.[164] T. M. Huh et al. fabricated a flexible capacitive pressure sensor using silicone for a robotic gripper [Figure 10b],[165] which has reconfigurable bumps to grasp wet and/or slippery objects.

5.4.2. Flexible Capacitive Pressure Sensors for Robotic Hands

Robotic hands, like the human hand, are used for grasping and gripping among other applications. M. Amit et al. presented a capacitive pressure sensor embedded glove for robotic hand [Figure 10c] for the purpose of minimizing humans in hazardous chemical analysis environments.[166] The flexible capacitive pressure sensor has PDMS foam as dielectric later and Ag + PDMS as conductive electrode.[166] The sensor is analyzed at different PDMS foam dielectric porosities with base capacitance of 4–8 pF for each sensor. The sensitivity for 85 vol% porosity of PDMS foam dielectric layer has 57 and 300 Pa⁻¹ for 3–20 kPa

**ADVANCED
SCIENCE NEWS**
www.advancedsciencenews.com

**ADVANCED
MATERIALS
TECHNOLOGIES**
www.advmattechnol.de

Figure 10. Flexible capacitive pressure sensor for robotics applications. a) Soft robotic puncture resistant gripper holding an object for material detection and sorting. Both fingers of the soft robotic gripper consist of flexible capacitive and strain sensors. Reproduced with permission.[163] Copyright 2019, IEEE. b) Soft robotic gripper; capacitive pressure sensors on the fingers have bumps to measure normal and shear pressure. Reproduced with permission.[165] Copyright 2020, IEEE. c) Schematics of robotic glove with capacitive pressure and chemical sensors designed for monitoring hazardous materials. Reproduced with permission.[166] Copyright 2019, RSC. d) 3D-printed robotic hand with biomimetic tactile sensor stack on index finger. Reproduced with permission.[167] Copyright 2019, Wiley. e) Soft robotic hand with integrated capacitive pressure sensors holding different materials Reproduced with permission.[168] Copyright 2018, IOP Science. f) 3D-printed robotic hand with soft flexible capacitive pressure sensors on each finger holding a stapler. Reproduced with permission.[169] Copyright 2020, Wiley. g) Flexible capacitive sensory robotic skin utilized for tactile sensing. Reproduced with permission.[170] Copyright 2016, IEEE. h) Capacitive pressure sensor array which is fabricated using simple micromachining process has micro-dome structure. Reproduced with permission.[174] Copyright 2019, IEEE. i) Robotic hand holding the fabricated flexible capacitive robotic skin and inset shows close-up view of the micro-bumps and electrodes. j) Robotic skin mounted on commercially available robotic gripper is used for tactile sensing by capacitance change which is monitored using LCR meter. (i,j)—Reproduced with permission.[110] Copyright 2018, AAAS. k) The soft robotic gripper composed of flexible and stretchable robotic skin with capacitive pressure sensors holding a wet and soft object. Reproduced with permission.[175] Copyright 2020, IEEE.

and <50 Pa pressure range, respectively.[166] W. Navaraj et al. presented biomimetic sensory stack with capacitive and piezoelectric tandem sensing structure on a 3D-printed robotic hand [Figure 10d] for tactile sensing to mimic human hand skin sensing.[167] The capacitive pressure sensor on the robotic hand reported static tactile sensing sensitivity of 250 and 2 Pa^{-1} at low (100 Pa) and high (2500 Pa) pressure range, respectively, however, nonlinear response is one major issue.[167] R. P. Rocha et al. incorporated a flexible capacitive pressure sensor on anthropomorphic soft robotic hand [Figure 10e] and analyzed the grasping process for four different objects.[168] The flexible capacitive pressure sensor was compared to a resistive pressure sensor and it was concluded that the capacitive sensor was better in terms of performance and physical properties.[168] M. Natagios et al. developed a 3D printed robotic hand and fabricated soft flexible capacitive pressure sensors using additive manufacturing technique with Ecoflex and polyurethane as dielectric layers. The sensors are placed for tactile sensing at the distal phalanxes of each of the five robotic fingers with each finger having the electronics embedded inside.[169] The 3D printed robotic hand is integrated with commercially available UR5 robotic arm and the actuation process was analyzed [Figure 10f] using commonly available laboratory objects, for example, stapler.[169]

5.4.3. Flexible Capacitive Pressure Sensory Skin for Robotics

Z. Ji et al. designed 4 × 4 flexible capacitive sensory robotic skin [Figure 10g] for measuring force range of 0–20 N full scale using copper as electrode and PDMS as dielectric material on PET substrate, for different types of robotic arm movement.[170] To increase the full scale pressure range for tactile sensing, various works presented flexible capacitive pressure sensor/skin using low-cost and easily available materials for 25,[171] 180,[172] 570,[173] and 1200 kPa[174] full scale pressure range. S. Wang et al. presented micro-dome structure based flexible capacitive pressure sensor [Figure 10h] using micromachining technique.[174] C. M. Boutry et al. presented a bio-inspired flexible and soft electronic robotic skin [Figure 10i] for normal and tangential pressure detection in which the substrate consists of micro-bumps and the bottom side of the pressure sensitive electrode consists of micro-grooves.[110] The connecting patches/interconnects are made of CNT-PU material and then the skin is mounted on a robotic arm [Figure 10j] to control movement and the capacitance data is recorded by LCR meter.[110] A. Gruebele et al. fabricated stretchable and flexible capacitive robotic skin for grippers [Figure 10k] which is unaffected by humid/wet environment, long-lasting, and highly sensitive to soft touch.[175] The sensory skin does not have any rigid components because the PCB, which converts capacitive to digital data, is mounted on the gripper itself.[175] H. S. Sonar et al. presented a capacitive pressure sensory soft and low-cost robotic skin which is fabricated using conductive fabrics and foam for pressure localization.[176] This work presents electrical and mathematical analysis performed for $n \times n$ matrix and the fabricated 1 × 5 and 5 × 5 matrix of soft deformable skin is experimentally characterized.

5.5. Wearable/Implantable Applications

Over the last two decades, wearable electronic devices have been trending due to the involvement and advancement of different research areas such as advanced manufacturing processes, computational mechanics, material technologies, miniaturization of different electronic components, and wireless communication.[177–179] Wearable sensors and actuators play a vital role from healthcare monitoring[42,121,180–186] and human-computer interaction[161,182,183,185–189] to consumer electronics applications.[185,186,190,191] Researchers utilized different fabrication techniques (i.e., both conventional and emerging) to design smart electronic skin which can be tagged/deployed/placed on different non-curvilinear surfaces for analysis of different parameters, including pressure.[121,192–196] Diverse applications of wearable flexible capacitive pressure sensors are reviewed for healthcare, human–computer interaction, and consumer/portable electronics.

5.5.1. Healthcare Applications

Flexible pressure sensors are one of the most integral part of any healthcare system and capacitive type is one which has been extensively explored as it plays a major role in measuring pressure at different locations on the body, not only on humans but also on animals, either by exterior placement (e.g., on skin) or by implantation, as discussed below.

Pulse Rate and Blood Pressure Monitoring: Flexible pressure sensors/e-skins have multiple applications in wearable systems, including monitoring pulse, heartrate, and blood pressure.[197–201] Arterial pulse rate is a key parameter for health monitoring, which is in range of 60–80 bpm (beats per minute) for adults. The pulse rate provides information about the heart and blood flow, specifically the frequency of heart contraction and expansion. The pulse rate varies from human to human and depends on body conditions, for example, pulse rate is higher while exercising. Various researchers have reported different approaches to monitor pulse rate using transistors and resistance/impedance change based flexible pressure sensors using new fabrication approaches which gained much attention.[187,200,202–206] Since the absolute pressure range of pulse rate is very small with low pressure amplitude, the flexible capacitive pressure sensor must have high sensitivity and highly linear response. B. C. K. Tee et al. designed flexible capacitive pressure sensors using micro-pyramids of different side wall angles as the dielectric.[106] The micro-pyramids sensor with maximum side wall angle is the most sensitive and is presented for different applications including pulse rate monitoring. The finger is placed at the designed sensor which can monitor only the systolic pressure [**Figure 11**a,b]. For continuous monitoring of pulse rate, the pressure sensor needs to be placed at an artery (e.g., at wrist, neck, behind knee, ankle joint) and should be compact to include miniaturized sensors with data acquisition (DAQ) system. B. Zhuo et al. monitored pulse rate (P, T, and D-waves) from 3D-printerd micro-structured PDMS mold based dielectrics with ITO as bottom electrode and PET as top electrode [Figure 11c,d].[207] For pressure range up to 0.2 kPa, the reported sensitivity of sensor was 1.62 kPa^{-1}. This proposed

ADVANCED
SCIENCE NEWS
www.advancedsciencenews.com

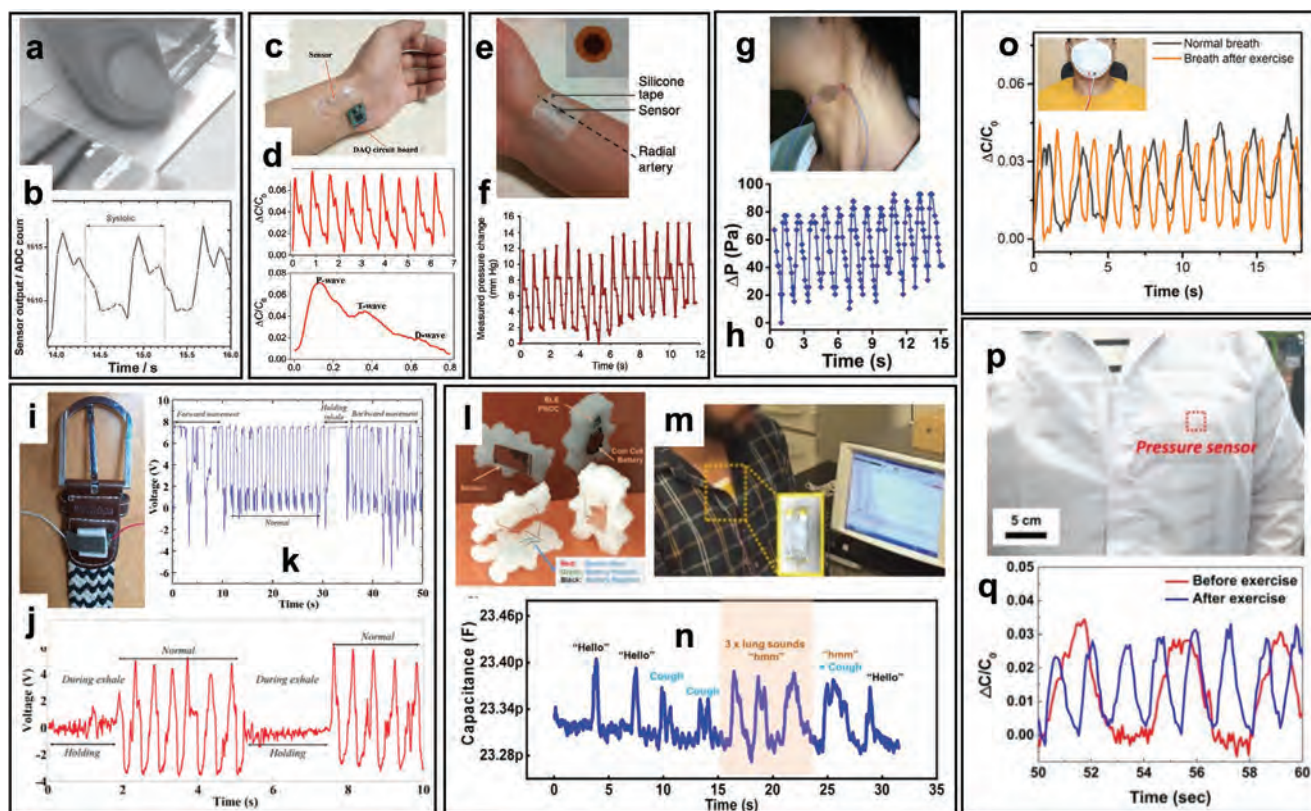ADVANCED
MATERIALS
TECHNOLOGIES
www.advmattechnol.de

Figure 11. Applications of flexible capacitive pressure sensors for pulse rate, blood pressure, and respiration monitoring. a,b) Fabricated flexible capacitive pressure sensor with micro-pyramid structured dielectric for finger pulse waveform monitoring. Reproduced with permission.[106] Copyright 2017, Wiley. c,d) Comprehensive sensory sensor system with DAQ board placed on the radial artery at wrist; pulse rate in one period (bottom) contains information of period (P)-wave, tidal (T)-wave, and diastolic (D)-wave. Reproduced with permission.[207] Copyright 2017, IEEE. e,f) Placement of a sensor on the radial artery of a subject to wirelessly monitor pulse rate. Reproduced with permission.[199] Copyright 2014, Nature Research. g,h) Placement of sensor on the neck near carotid artery for continuous monitoring of blood pressure. Reproduced with permission.[115] Copyright 2020, RSC. i) Photograph of pressure sensor attached to the backside of belt. j) Real time respiration signal monitoring of 3rd subject. k) Real time monitoring of first subject in forward and backward bending postures. (i–k)—Reproduced with permission.[213] Copyright 2017, IEEE]. l) Metal-coated polymer and paper-based flexible capacitive pressure sensor packaged using Styrofoam with wireless PSoC-BLE system on the backside of sensor. m) An attached sensor on chest of human subject for real-time monitoring. n) Real time data acquisition from the chest of a human subject. (l–n)—Reproduced with permission.[42] Copyright 2020, IEEE. o) Respiration rate monitoring using pressure sensor on mask before and after exercise. Reproduced with permission.[212] Copyright 2020, ACS. p,q) Respiration rate monitoring before and after exercise with sensor placed on the chest of subject. Reproduced with permission.[28] Copyright 2020, RSC.

architecture of sensor and DAQ circuitry are well developed, however in this modern era, there is requirement for wireless data transfer which can be recorded on mobile phone/tablets or at nearby hospitals. L. Y. Chen et al. presented in vivo monitoring of pulse rate with a complete system consisting of flexible capacitive pressure sensor and flexible antenna[Figure 11e].[199] The subject had 82 bpm heart rate which is monitored for 12 s time duration with resolution of 90 ms [Figure 11f].

The normal range of blood pressure is less than 120 mmHg systolic and 80 mm Hg diastolic. In the case of high blood pressure (i.e., hypertension), the systolic and diastolic blood pressure varies from 120 to 160 mm Hg and 80 to 100 mm Hg, respectively, which increases the possibility of cardiovascular or kidney disease.[6,63,208,209] A transparent and micro-droplet glyoxal dielectric based capacitive pressure sensor is presented for continuous blood pressure monitoring by B. Nie et al.[115] The flexible capacitive pressure sensor is placed on the neck (near carotid artery) and monitors blood pressure [Figure 11g] with

response time of 100 ms, resolution of 1.8 Pa, and mechanical-to-electrical sensitivity of 1.58 μF kPa^{-1} [Figure 11h]. The reported sensor can be utilized for other biomedical systems like ocular, pulmonary, and cardiovascular as it detects pressure in range of 2–10 kPa.

Respiration/Wheezing Monitoring: Respiration monitoring in everyday can provide early detection of several diseases like emphysema, bronchitis, asthma, and sleep apnea.[210–212] Continuous monitoring of respiration can save human lives and is actually very common for athletes, and nowadays, even normal people.[213] Several researchers proposed monitoring respiration or wheezing using flexible capacitive pressure sensors. S. W Park et al. fabricated a flexible capacitive pressure sensor and placed it on the backside of a commercially available waist belt [Figure 11i].[213] The sensor is attached with the signal conditioning circuitry to convert the capacitance into voltage, which then passes through a low pass filter (cut off frequency = 20Hz), instrumentation amplifier, and

analog-to-digital convertor. Afterward, noise and interference are removed with the help of a MATLAB-coded finite element response (FIR) based filter. Real time signal monitoring is performed for inhale, exhale, and the hold time between by three different subjects while body is straight, that is, no bending of sensors. The response of third subject is shown in Figure 11j. The sensor is also characterized for forward and backward body movements and voltage peaks show amazing repeatability [Figure 11k]. The sensor demonstrates excellent response of continuous respiration rate monitoring, however wearing bulky signal conditioning and DAQ circuitry can be uncomfortable. S. M. Khan et al. designed diaphragm-based flexible capacitive pressure sensors from metal coated polymer and double-sided tape for asthma monitoring [Figure 11l].[42] Different diaphragm shapes (circular, square, and rectangular) have been analyzed to choose the shape that is most sensitive; finite element analysis determined it to be the circular. Three different sounds (man, woman, and baby) were chosen for characterization and a standalone system was designed to report the change in capacitance for each sound.[42] For real-time respiration monitoring, the sensor was placed on the chest of an adult (29-year-old) subject [Figure 11m] who makes different sounds like "hello" and lung sounds [Figure 11n].

S. Sharma et al. performed respiration monitoring of breathing before and after exercise using composite nanofibrous scaffolds based flexible capacitive pressure sensors.[212] The sensor is attached to a mask worn by the subject (healthy 30 years old) for respiration monitoring which shows increase from 24 to 48 respiration cycles per minute for before to after exercise [Figure 11o]. The sensor shows excellent response; however, as masks are not worn constantly, a more practical system needs to be designed, such as sensor embedded in textile clothing or stuck on the chest, for respiration monitoring. G.-K. Jeon et al. presented a flexible capacitive pressure sensor with PDMS/Ecoflex solution as dielectric material and spray-coated silver nanowire (AGNW) as electrode for respiration monitoring before and after exercise. The sensor is attached to the subject's chest for respiration rate monitoring [Figure 11p] and the respiration cycles [Figure 11q].[28]

Foot Plantar Pressure Monitoring: Biomechanical analysis of gait recognition and posture relies on the study of pressure between the plantar surface of foot and floor, known as pedobarography.[214] Plantar pressure measurements can also aide in the diagnosis and treatment of foot injuries, deformations or balance, and confirm effectiveness of treatments or orthotics. Gait analysis in clinical science became revolutionized by the ability to study pressure distributions on feet during static and dynamic motion.[214,215] Different approaches are proposed across several research areas including MEMS,[216,217] fiber-optical sensor,[218] artificial neural network,[215,219] and deep learning.[220] Flexible capacitive pressure sensors are also being utilized for analyzing foot plantar pressure. The sensors need to be very robust and applicable for high pressure range. K. F. Lie et al. presented a flexible capacitive pressure micro sensor which has bumps and PDMS dielectric layers,[221] fabricated using micromachining technology with an operating range of up to 945 kPa and 6.8% per N.

Instead of using a sensory matrix for plantar pressure measurement, the insole type wearable system is claimed as most suitable configuration and has become popular among different researchers. S. W. Park et al. designed a smart insole system which can analyze gait using signals from right and left foot during motion.[222] The large area sensors are fabricated using emerging fabrication technologies with electrodes composed of MWCT/PEDOT:PSS and dielectric material of porous PDMS. The fabricated sensor is inserted into a heel of commercially available shoe insole and connected to signal conditioning circuitry designed using an amplifier. A low-pass filter reduces noise and interference as part of the signal conditioning circuitry and then the signal passes to a MATLAB program for voltage measurement. To demonstrate real time monitoring, the subject walks with speed of 4.9 m s^{-1} with findings shown in **Figure 12**a. The alternating peaks from left and right foot signals correspond to the walking motion. This work is well presented however it did not include the pressure distribution of whole foot. J. Tao et al. designed a smart insole system for real time monitoring of planter pressure.[223] Figure 12b shows fabrication steps of the 24 sensory array system in which the bottom electrode is patterned using a laser and the same pattern is employed for Ecoflex elastomer dielectric layer. The top electrode is placed on the dielectrics to make the capacitive pressure sensor array and an additional shielding layer is on top of that. The planter pressure is monitored for four different yoga postures (static pressure monitoring) and different ways of walking (dynamic pressure monitoring) in which the analyzed capacitance change correlates to the pressure applied on the feet [Figure 12c,d].

Intraocular and Intracranial Pressure Monitoring: Increased fluid pressure in the eye increases risk for developing glaucoma. Glaucoma being any eye condition that could damage the optic nerve. Measuring eye fluid pressure can help with early detection of glaucoma and treatments for glaucoma include reducing eye fluid pressure intraocular pressure (IOP) (normal range: 1.6–2.8 kPa). This disease requires continuous real time monitoring using cost-effective devices. The "Goldmann Applanation Tonometer" is the conventional device used to measure IOP.[49,224–227] However, for continuous IOP monitoring, different approaches have been presented, such as impedance measurement technique[228,229] that can be utilized like contact lenses, or whole microsystems[230] that can be implanted inside a patient's eye. Nevertheless, several challenges for this sensing application have been reported including sensor flexibility, high system costs, availability of contact area, and biocompatibility. D. Ha et al. microfabricated a flexible capacitive pressure sensor while considering all these challenges.[26] The sensor has a square pressure sensitive diaphragm (area = $300 \times 300\ \mu m^2$ and thickness = $30\ \mu m$) which can operate across 0–50 mmHg pressure range with high linear response and sensitivity of 0.3 fF per mm Hg [Figure 12e]. The sensor is experimentally demonstrated for real time monitoring on a round surface that mimics a mouse eye [Figure 12f,g].

Intracranial pressure (ICP) arises due to head injuries or diseases like brain tumors or chronic hydrocephalus.[231–234] Since the brain has a very complex structure, implantation of sensors with corresponding signal conditioning circuitry is one of the
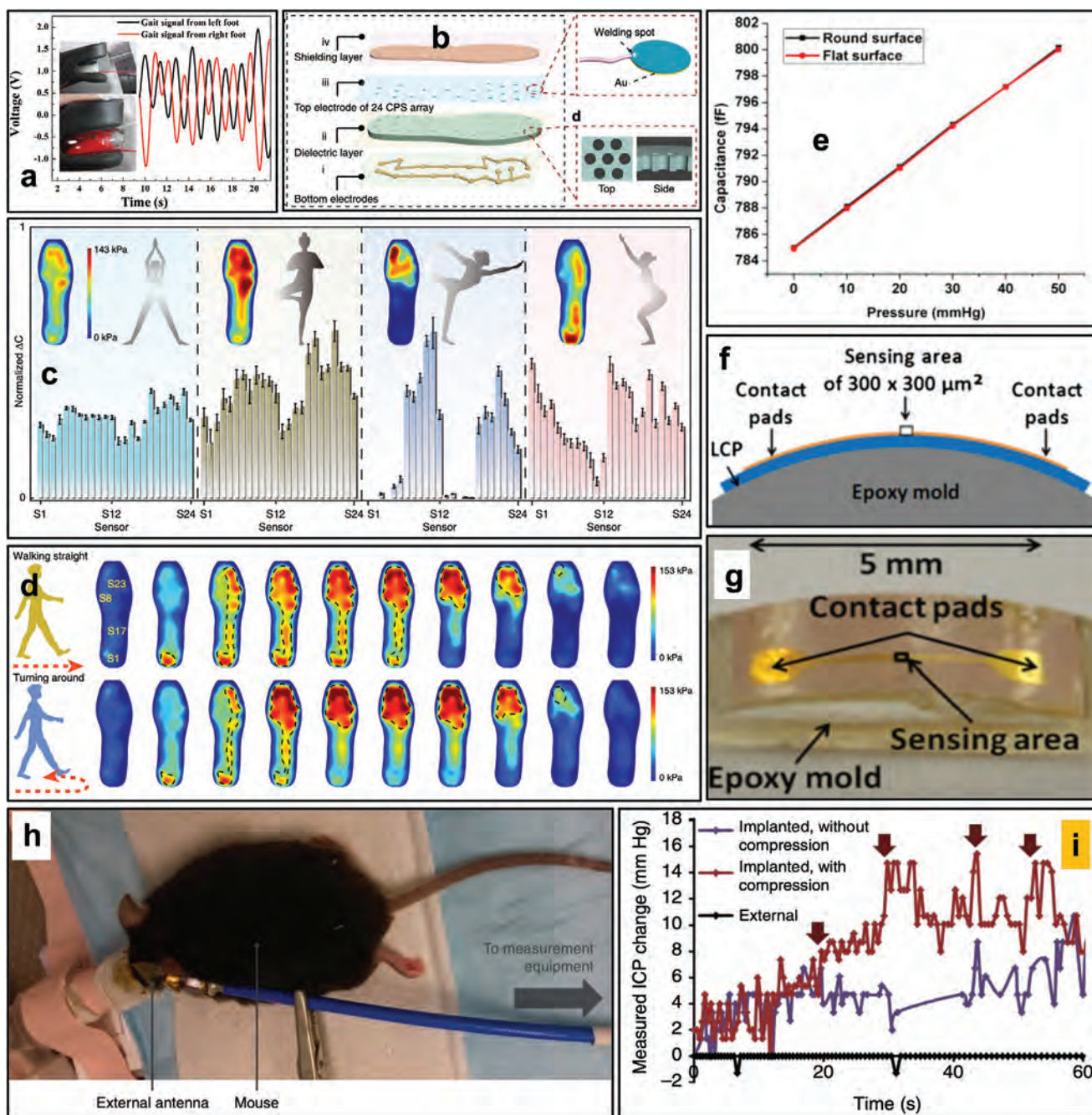
Figure 12. Applications of flexible capacitive pressure sensors for plantar, intraocular, and intracranial pressure monitoring. a) Response of left and right foot plantar pressure for fabricated insole system placed inside the backside of shoe. Reproduced with permission.[222] Copyright 2018, Elsevier. b) Fabrication steps of Ecoflex silicone elastomer based flexible capacitive sensor matrix of 24 sensors designed for insole plantar pressure monitoring system. c) Monitoring plantar pressure-measurement from fabricated sensory matrix for four different yoga postures (static condition). d) Monitoring of plantar pressure when walking (dynamic condition). (b–d)—Reproduced with permission.[223] Copyright 2020, Nature Research. e–g) Response of flexible capacitive pressure sensor (area = 300 × 300 μm²) measured on curved surface to mimic a mouse eye for real time monitoring. Reproduced with permission.[26] Copyright 2011, Springer. h,i) The pressure sensor is implanted inside mouse eye and the antenna is placed on mouse brain. Response of sensor is measured for 60 s duration with and without compression on brain of mouse and compared with an external reference sensor. The arrows are shown to indicate when compression was applied on brain of mouse. Reproduced with permission.[199] Copyright 2014, Nature Research.

challenges reported by different researchers. A capacitive pressure sensor with inductive coil is being utilized to transmit the ICP measurement via wireless communication. Q. Wei et al.

microfabricated a flexible capacitive pressure sensor placed at the center of an inductor coil which can be implanted inside human brain for continuous real time monitoring of ICP.[235]

**ADVANCED
SCIENCE NEWS**
www.advancedsciencenews.com

**ADVANCED
MATERIALS
TECHNOLOGIES**
www.advmattechnol.de

The pressure sensor is characterized using air pressure setup for 0–10 kPa pressure range providing a plot of capacitance and frequency versus intracranial pressure. For real time ICP sensor characterization, L. Y. Chen et al. fabricated flexible LC-system for continuous in vivo monitoring of ICP[199] demonstrated by implanting the system in a mouse brain [Figure 12h]. The compression inside the mouse brain increases the ICP and as compression in brain increases, the increment in pressure mapping from baseline also increases [Figure 12i].

5.5.2. Consumer/Portable Electronics Applications

Several applications for capacitive pressure sensors in the areas of consumer and portable electronics have been demonstrated, including keyboard, object detection, hand gesture detection, and weight estimation. Such applications require highly sensitive and fast pressure sensors that can be fabricated using simple processes. R. Shi et al. demonstrated a skin-wearable keyboard using an array of 55 transparent pressure sensors which can differentiate the applied pressure on individual pixels.[190] The pressure sensors used a composite material of silver nanowires and PDMS as the dielectric. The dielectric was also patterned into pyramidal shapes in order to enhance the sensor sensitivity. By sandwiching the dielectric composite between ITO/PET sheets, a large sensitivity of 0.831 kPa^{-1} is obtained with a low detection limit of 1.4 Pa. The pressure sensor also exhibited a fast response time of less than 30 ms with a relaxation time of less than 60 ms. The authors confirmed the reliability of the sensor using a 10k cycling test. By arraying 5 × 5 sensors, the authors demonstrated a functional keyboard which was able to type the letter "f" and word "Flextronics" by simply detecting the capacitance variation of each pixel. To achieve this, the sensor array was integrated into a complete system, which included switching and oscillating circuitry, microprocessor, and wireless transmission unit [**Figure 13**a]. The oscillating circuitry detects the capacitance change of the sensors while the microprocessor determines the pixel information which is then sent wirelessly to mobile phone software.

K. Lee et al. demonstrated a low-cost paper-based 3D touchpad.[236] The pressure sensors are based on graphite electrodes developed using pencil writing on a paper. The electrode was then coated with a thin PDMS layer which preserves the surface roughness of the graphite/paper stack. A similar electrode layer is then formed and added on top of the first stack. As a result, a rough structured PDMS layer is sandwiched between graphite electrodes formed on paper substrate. The resulting pressure sensors exhibited a sensitivity of 0.62 kPa^{-1} with fast response and relaxation times (hundreds of milliseconds), in addition to a low detection limit of 6 Pa. The authors confirmed the reliability of the sensors using cycling tests of repeated loading (5k) and bending (1k). By arraying 3 × 3 sensors, the authors demonstrated the ability of the array to detect the capacitance change in each sensor when soft and hard touches are performed [Figure 13b]. The same fabrication technique is utilized to design keyboard which consists 27 pressure sensor which includes all the alphabets and space bar, and thus typing the words "Yonsei University"

was possible. In another work, S. Takamatsu et al. were able to demonstrate the application of a keyboard based on capacitive pressure sensors fabricated on knitted textile using PEDOT:PSS electrodes.[237] The sensors could detect pressures down to 0.05 N cm^{-2} while the keyboard showed stretchability of 30%. Nevertheless, the response time and sensitivity of the devices were not reported.

Employing the same principle used in keyboard application, the application of capacitive pressure sensors for object detection has been demonstrated. In this case, the change in the measured capacitance over an array of sensors allows the detection of the object location and stiffness. X. Wang et al. developed a flexible and stretchable 3 × 3 sensory array capable of detecting object morphology and stiffness.[238] Using a parallel plate electrode with serpentine design and PDMS as the dielectric material, the sensors exhibited 90% stretchability and a near zero temperature coefficient while the response time was limited to an embedded microchip with 90 Hz frequency. It should be noted that the PDMS dielectric was also designed to show micropillar structures with 200 μm height and 10 μm diameter in an attempt to improve the tactile sensitivity and lower detection limit of the sensors [Figure 13c]. The authors demonstrated the ability of the 3 × 3 sensor array to differentiate between an apple and an orange when placed on top of the array [Figure 13d]. C. Metzger et al. used flexible polyolefin foam as the dielectric material to achieve ultra-low-cost capacitive pressure sensors (0.9$ per meter) with moderate sensitivity and load resolution of less than 10 g cm^{-2}.[90] However, the authors mentioned that the sensitivity is large enough to perform object detection where an array of the sensors was capable of differentiating between three distinct objects based on their weight and morphology.

In order to achieve higher sensitivity, Y Luo et al. proposed a capacitive pressure sensor using tilted micropillars of PDMS as the dielectric material.[111] The tilted micropillars enable a bending deformation rather than compression deformation which results in larger changes of distance between the electrodes upon pressure application. As a result, a high sensitivity of 0.42 kPa^{-1} with a low detection limit of 1 Pa and an excellent stability after 1k cycles are reported. It is worth noting that the tilted micropillars were developed by coating PDMS onto a tilted exposure photoresist mold and that the tilt angle can be customized by modifying the exposure angle. By integrating several sensors on a glove, the set was able to detect different finger and hand gestures [Figure 13e]. Moreover, X Liang et al. used an array of 5 × 1 capacitive pressure sensory skin around a wrist to detect hand gestures.[239,240] In this case, however, the authors used commercial capacitive sensors which were then encapsulated using PDMS and placed around the wrist. The measured capacitance changes due to the tendon movements were fed into a system with machine learning capabilities which allowed for over 90% real-time gesture recognition. Finally, the pressure sensors have also been used in application of detecting the weight of wearable objects, such as a backpack, where capacitive pressure sensors were integrated on the backpack strap.[241] The sensors used a dielectric material based on porous PDMS with a mixture of NaHCO$_3$ and HNO$_3$. The silver electrodes were then fabricated using screen
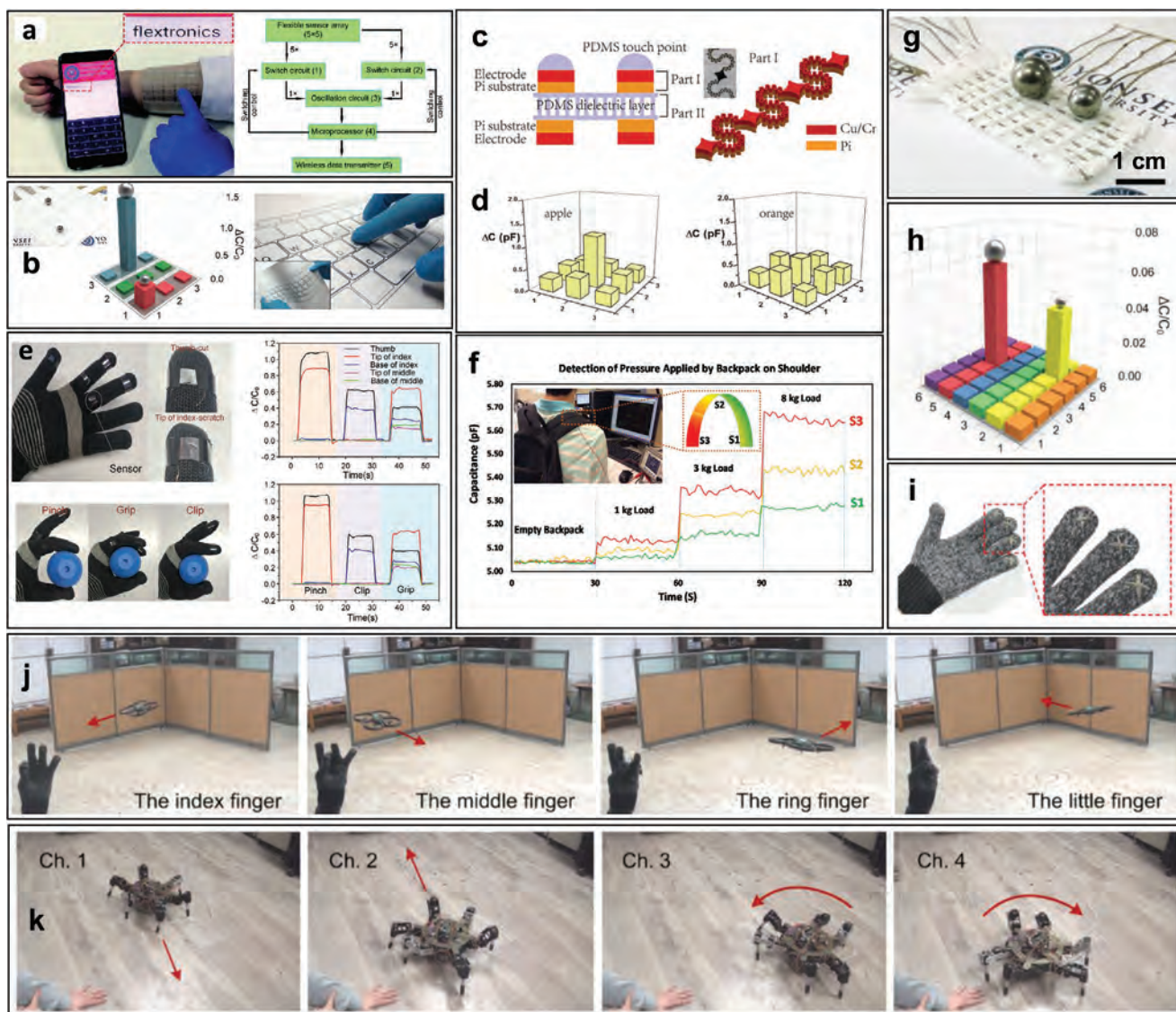
Figure 13. Applications of flexible capacitive pressure sensors for consumer and portable electronics. a) Demonstration of real-time typing of the word "flextronics" using the flexible keyboard based on capacitive pressure sensor with AgNWs/PDMS composite as the dielectric material. Complete system components are shown on the right. Reproduced with permission.[190] Copyright 2018, Springer. b) Photograph of the 3×3 multiple-pixel pressure sensor array based on graphite electrodes formed on paper substrate. The reconstructed map with various column heights shows the relative capacitance change when two balls with weights of 5 and 50 g are placed on the array. Same fabrication technique is utilized to design the keyboard which is formed on paper substrate. Reproduced with permission.[236] Copyright 2017, Wiley. c) The cross-sectional illustration of the pressure sensor using a parallel plate of serpentine electrodes and micropillar-based PDMS dielectric. d) The reconstructed map of the capacitance changes measured by 3×3 sensory array when an apple and orange are placed on the array. (c,d)—Reproduced with permission.[238] Copyright 2017, RSC. e) Gloves with five integrated sensors on the fingers are capable of detecting the fingers and hand gestures as shown in the measured capacitance change plots. The sensors are based on parallel plate capacitors with tilted PDMS micropillars as the dielectric material. Reproduced with permission.[111] Copyright 2019, ACS. f) Detection of backpack weight using porous PDMS based capacitive pressure sensors with screen printed silver electrodes. The 3×1 sensory array is attached on the backpack strap using a heat press lamination process. Reproduced with permission.[241] Copyright 2019, IEEE. g,h) Fabricated 6×6 flexible pressure sensor array from Kevlar fiber as dielectric with AgNP/SBS composite electrode and response of 2×5 and 5×5 number sensor under 0.25 and 0.87 g beads. i,j) Kevlar fabric dielectrics based four flexible pressure sensor pressure sensors are attached with gloves on the on the tips of index, middle, ring, and smallest finger, which is utilized to control the drone. k) Same set of four pressure sensors are incorporated on the hoody to control the hexapod robot. (g–k)—Reproduced with permission.[120] Copyright 2015, Wiley.

printing and the devices were attached on the fabric of the backpack using heat press lamination. The sensors showed a short response time of 0.8 s with the capability to detect a wide range of pressures varying from 0 up to 900 kPa. Different pressure ranges resulted in different sensitivities where

the largest measured sensitivity of 0.8% kPa^{-1} was observed for the pressure range of 50–200 kPa. By integrating three sensors on the strap of the backpack, the array was able to detect the weight of the backpack when loads up to 8 kg are added [Figure 13f]. Moreover, J. Lee et al.[120] presented the Kevlar

Table 1. Performance comparison between different operation modes of flexible capacitive pressure sensors with air dielectric, as discussed in this review.

Mode/shapes		Dielectric thickness [µm] (approx.)	Overlapping area [cm²]	Operating pressure range [Pa]	Mechanical sensitivity [µm Pa⁻¹] (simulation)	Rise time [ms]	Ref.
NMCPS	Cantilever	250	0.15	0–1	62	75	[39]
	Rectangular	350	π	0–40	0.0776	—	[41]
	Square	350	π	0–40	0.0815	—	[41]
	Pentagon	350	π	0–40	0.104	—	[41]
	Ellipse	350	π	0–40	0.867	—	[41]
	Circle	350	π	0–40	1.163	—	[41]
TMCPS		400	π	0–50	—	≈ 15.85	[81]
DTMCPS		451	π	0–60	—	≈ 16	[84]

fabric dielectric-based 6 × 6 capacitive pressure sensory array is fabricated and characterized using two weight beads of 0.25 and 0.87 g [Figure 13g,h]. The four sensors are incorporated on the clothes (gloves and hoody) for wireless controlling of drones and hexapod robots [Figure 13i,k].

6. Conclusions and Outlook

In this paper, the latest flexible capacitive pressure sensors are reviewed from the perspective of operation principle, materials, fabrication techniques, and applications. In general, capacitive pressure sensors are based on a parallel plate capacitor structure with an embedded dielectric. By applying perpendicular pressure to the electrodes, the distance between them changes resulting in a change in the measured capacitance. While elastomeric dielectrics have been widely used in flexible capacitive pressure sensors due to their inherently ultra-flexible nature, the sensitivity of such sensors is limited by the compressibility of the rubbers. Thus, to achieve highly sensitive flexible pressure sensors, researchers have proposed several approaches for optimizing the dielectric layer by using air, micropillars and microstructures, embedding AgNWs or composite materials into the flexible dielectric layer, printed materials, fabrics, fibers, or coating the surface of the dielectric layer with nanomaterials. Moreover, various designs and materials have been studied for the electrodes in order to enhance their flexibility and stretchability, such as using fractal designs (e.g., serpentine structure) or inherently flexible and stretchable conductive materials (e.g., CNTs or metallic nanoparticles embedded in elastomers). Additionally, capacitive pressure sensors can achieve high transparency and biocompatibility when the electrodes are replaced with ionic conductors that generally exhibit excellent stretchability and stability. Such structures are promising for ionic skin applications. Each of these dielectric materials and designs uniquely affect performance parameters and operating range of sensors, which are decisive to their application, and are summarized in **Tables 1** and **2**.

In terms of fabrication approaches, several methods have been studied ranging from low-cost techniques, such as simple graphite coating on paper substrate using a pencil, to more sophisticated techniques that allow for miniaturization using micro- and nano-fabrication tools, such as photo- and e-beam lithography to achieve micro-pillars or nanomaterial-based dielectrics. Nevertheless, there is usually a tradeoff between the different traits of the flexible pressure sensors, such as cost, sensitivity, scalability, or reliability. Capacitive pressure sensors are generally characterized by detecting capacitance change upon pressure application where the main figures of merit include sensitivity, response time, relaxation time, lower detection limit, reliability in terms of cycling, maximum flexibility, and stretchability (%). Researchers are encouraged to report these values in their future studies for a better understanding and benchmarking of capacitive-based flexible pressure sensors.

Flexible capacitive pressure sensors have been demonstrated over a wide range of applications, including: altitude, air, and wind speed monitoring in the aerospace industry; tire pressure, gas exhaust regulation, and airbags in the automotive industry; sea depth in the marine industry; e-skins, robotic grippers, and hands in the robotics industry; pulse rate, blood pressure, plantar pressure, and respiration monitoring in the healthcare sector; hand gesture, object, and weight detection, and keyboards in the consumer and portable electronics sector. This wide range of essential applications shows the importance and the need to further enhance the performance of current flexible pressure sensors using lower cost techniques.

Finally, a capacitive pressure sensor detects input from the outer environment and produces an electrical signal that is then treated and converted into an informative output to the end user depending on application. The signal processing circuitry should be designed to meet the specific requirements of a given application. Therefore, not only the performance and fabrication costs of the pressure sensors, but also signal transmissivity, costs of integrating sensors into a complete system, and stability are challenges that need to be tackled in order to fully evolve from proof-of-concept devices fabricated in laboratory to reliable complete systems used in our daily life.

Table 2. Performance comparison between flexible capacitive pressure sensors with different designs and dielectric and electrode materials, as discussed in this review.

Type of flexible capacitive pressure sensor	Dielectric material	Electrode material	Dielectric thickness [μm]	Operating pressure range [kPa]	Maximum sensitivity [kPa^{-1}]	Pressure range for maximum sensitivity [kPa]	Response time [ms]	Ref.
Graphene and graphene-based materials	Graphene and porous nylon n/w	Ag	≈ 34	0–5	0.33	0–1	<20	[86]
	Branched-CNTs and GNPs (3:1)	Ag	≈ 800	0–1.2 × 10^3	≈ 2.05 × 10^{-3}	0–1.2 × 10^3	—	[89]
	Graphene oxide (GO)	PET	≈ 300	0–4	≈ 0.8	0–1	≈ 100	[88]
Elastomers/foam/sponge/composites	Polyolefin foam	—	250	0–1.029	≈ 8.25 fF	0–1.029	—	[90]
	PDMS	Cu	30	0–945	0.0019	0–945	—	[221]
	Ecoflex	CNT	≈ 500	10–150	5.9 × 10^{-4}	10–150	—	[242]
	PDMS/Parylene–C	Pt/Au	11	0–140	0.024	0–10	—	[243]
	PDMS	Cu	90	240–1000	0.22 × 10^{-4}	240–1000	—	[244]
	Ecoflex	CNT	500	1–1400	0.0016	0–500	≈ 40	[245]
	PDMS	AgNW	≈ 500	0–260	4.0 × 10^{-4}	0–50	—	[246]
	PU sponge	AgNW	—	0–70	5.54	0–0.03	—	[247]
	Porous PDMS	ITO	100	0–5	1.18	0.02	150	[248]
	40 wt% PDMS	Graphite on paper	6	0–10	0.62	0–2	200	[236]
	CaCu$_3$Ti$_4$O$_{12}$–PDMS sponge	—	4	0–1.3	1.66	0–0.64	33	[249]
	PDMS/SiO$_2$ beads	PEDOT:PSS	PDMS—5 and SiO$_2$ beads—6 to 9	0–11	1	0–11	140	[250]
	Porous PDMS	ITO/PET	15	0–40	0.759	<5	230	[93]
	Graphene/PDMS sponge	Cu	—	0–500	0.12	1–10	≈ 7	[87]
	Silicone	Conductive fabric	960	0–100	0.0121	—	7	[92]
	PDMS	AgNPs/CNTs	500	0–45	0.0486	0–15. 601	<50	[251]
	PU sponge	ITO/PET	50	0–116	5.3 nF	0–116	—	[252]
	PDMS/Ecoflex	AgNW	3	0–80	0.16 ± 0.03	0–1	70	[28]
	PDMS	ITO/PET	3	0–216	8.3	0.022	—	[253]
	Carbon black/PDMS/PET	Conductive carbon tape	1210	0–5	35	0–0.2	—	[254]
	PDMS/microsphere composite	ITO/PET	—	0–150	0.124	0–15	167	[255]
	Ecoflex silicone elastomer (porous)	Laser patterned	600	0–200	0.012	0–200	132	[223]
	PDMS	Micro-patterned Au	4	0–9	30.2	0–0.13	25	[256]
Wrinkled dielectrics	PMMA or PVP	AgNW and Ag	—	0–4.5	3.8	0–0.5	<150	[99]
	Wrinkled PDMS	Ag	—	0–10	19.80%	0–10	<200	[102]
	Wrinkled μ-arrayed PDMS	AgNW	—	0–6.7	2.94 ± 0.25	0–2	<50	[37]
	Wrinkled μ-arrayed PDMS	AgNW	—	0–9	2.04 ± 0.16	0–2	<100	[101]
	Wrinkled μ-structures Ecoflex	Au	—	0–8	0.0012	0–1	578	[98]
	Wrinkled μ-structures PDMS	Ti/Au	—	0–40	14.268	0–0.7	<50	[100]

Table 2. Continued.

Type of flexible capacitive pressure sensor	Dielectric material	Electrode material	Dielectric thickness [μm]	Operating pressure range [kPa]	Maximum sensitivity [kPa^{-1}]	Pressure range for maximum sensitivity [kPa]	Response time [ms]	Ref.
Micro-pyramids and micro-bumps	PDMS μ-pillars	ITO/PET	−6	0–7	0.55	0–2	<<10^3	[105]
	PDMS μ-pillars	Al	34	0–22	—	—	—	[106]
	PDMS μ-structure	Ti/Au and PET/ITO/Parylene	24.7	0–0.35	70.6	0–50	—	[107]
	PDMS μ-pyramid	Ag/PET	1500	0–10	2.21	0–0.1	50	[108]
	Ionic gel μ-pyramids	PET/ITO	5	0–0.5	41.64	0–0.4	<20	[109]
	PHB/PHV	CNT/PU	10	0–350	0.19 ± 0.07	0–1	—	[110]
	PDMS μ-structure	Ni/Ti and SWNT	—	0–25	0.7	0–25	50	[257]
	PDMS hierarchically μ-structured	Pt	—	0–100	≈ 3.73	0–0.1	21	[258]
	Ultraviolet-curable adhesive/graphene	Graphene	15	0–4	7.68	0 to ≈0.5	30	[36]
	PDMS μ-pyramids	Ti/Au	≈140	0–2.5	0.16	0–0.75	346	[259]
	PDMS μ-arrays	Au	50	0–12	4.9	0–2.5	<50	[188]
	Thermally expandable microsphere/PDMS			0–50	0.201	0–4500	60	[260]
	PDMS μ-structures	ITO/PET	—	1–3.5	1.62	0–0.2	—	[207]
	Spiky Ni/PDMS composite	75% wt Ag microflakes/PDMS	—	0–500	1.149	0–20	50	[261]
	PDMS tilted μ-pillars	Au/PET	—	0–14	0.42	0 to ≈ 2	<20	[111]
Fluidic/ionic liquid dielectrics	PVA/H$_3$PO$_4$ GIA	Au	—	0–360	3302.9	0–10	9	[112]
	PVDF/ionic liquid	AgNW	200	0–120	1.194	0–0.5	40	[114]
	Electrolyte/glycerol	ITO	—	—	1.58 μF	—	260	[115]
	Barium strontium titanate/Hg droplet	Al	1.501	0–3	2.24 μF	0–3	—	[262]
	Imidazolium-based ILs	ITO	—	—	0.43 nF	—	—	[116]
	Nafion solutions	ITO	50	0–30	5 nF	0–5	—	[117]
	Ionic alginate hydrogel (IAH)	PET with Ag-patterns	300 ± 5	—	9.32%	—	—	[118]
	1-Butyl-3-methylimidazolium bis-(trifluoromethyl)-imide	PET/ITO	—	0–18	178.5 nF	7–18	30	[114]
Fiber dielectrics	Kevlar	AgNP/SBS	—	0–10	0.21	0–2	—	[120]
	Twaron	AgNP/SBS	—	0–50	0.278	0–2	340	[119]
Printed dielectrics	PDMS	Ag	200	800–1.8 × 10^4	—	—	—	[124]
	PDMS	Ag	200	200–2400	—	—	—	[125]
	P(VDF–TrFE)	Ag paste	3	3.3 × 10^4–5.5 × 10^4	—	—	—	[126]
	PDMS	CNTs ink	1150	1.52–337	0.021	1.52–337	—	[127]
	CNTs/PDMS	Ag ink	68	0–850	2.9	0–450	—	[128]
	Regular thermoplastic-TPU	Conductive thermoplastic-TPU	200	1.5 × 10^4–3 × 10^4	5 × 10^{-5}	—	—	[129]
	PI/air	Silver ink	1000	1–1 × 10^5	16.7 pF per bar	—	—	[130]

[1] D. N. Doebelin, O. Ernest, Manik, *Measurement Systems: Application and Design*, Tata McGraw Hill, New Delhi **2007**.

[2] R. B. Northrop, *Introduction to Instrumentation and Measurements*, CRC Press, Boca Raton, FL **2017**.

[3] M. A. Nour, M. M. Hussain, *Sensors* **2020**, *20*, 3907.

[4] R. B. Mishra, S. S. Kumar, R. Mukhiya, in *Advances in VLSI, Communication, and Signal Processing - Select Proceedings of VCAS 2018*, Lecture Notes in Electrical Engineering (Eds.: D. Datta, H. Kar, C. Kumar, V. Bhadauria), Springer, Singapore **2020**, pp. 497–506.

[5] S. S. Kumar, B. D. Pant, *Microsyst. Technol.* **2014**, *20*, 1213.

[6] R. B. Mishra, S. S. Kumar, R. Mukhiya, in *Recent Trends in Communication, Computing, and Electronics*, Lecture Notes in Electrical Engineering (Eds.: A. Khare, U. Tiwary, I. Sethi, N. Singh), Springer, Singapore **2019**, pp. 441–449.

[7] G. K. Ananthasuresh, L. L. Howell, *J. Mech. Des. Trans. ASME* **2005**, *127*, 736.

[8] R. B. Mishra, S. S. Kumar, *J. Phys. Conf. Ser.* **2019**, *1240*, 012068.

[9] J. W. Judy, *Smart Mater. Struct.* **2001**, *10*, 1115.

[10] N. El-Atab, S. F. Shaikh, S. M. Khan, M. M. Hussain, *Adv. Eng. Mater.* **2019**, *21*, 1900043.

[11] N. El-Atab, R. Almansour, A. Alhazzany, R. Suwaidan, Y. Alghamdi, W. Babatain, S. F. Shaikh, S. M. Khan, N. Qaiser, M. M. Hussain, *Small* **2020**, *16*, 1905399.

[12] A. E. Kubba, A. Hasson, A. I. Kubba, G. Hall, *J. Sens. Sens. Syst.* **2016**, *5*, 95.

[13] K. N. Bhat, *J. Indian Inst. Sci.* **2007**, *87*, 115.

[14] S. M. Ahmed, A. M. Hussain, J. P. Rojas, M. M. Hussain, in *Proc. IEEE Int. Conf. Micro Electro Mechanical Systems*, IEEE, Piscataway, NJ **2014**, pp. 548–551.

[15] G. T. Sevilla, J. P. Rojas, S. Ahmed, A. Hussain, S. Bin Inayat, M. M. Hussain, in *2013 Transducers Eurosensors XXVII 17th Int. Conf. Solid-State Sensors, Actuators Microsystems (TRANSDUCERS EUROSENSORS XXVII)*, IEEE, Piscataway, NJ **2013**, pp. 2636–2639.

[16] J. M. Nassar, A. M. Hussain, J. P. Rojas, M. M. Hussain, *Phys. Status Solidi* **2014**, *8*, 794.

[17] M. M. Hussain, N. El-Atab, *Handbook of Flexible and Stretchable Electronics*, CRC Press, Boca Raton, FL **2019**.

[18] A. M. Hussain, M. M. Hussain, *Adv. Mater.* **2016**, *28*, 4219.

[19] M. M. , Hussain, J. M. Nassar, S. M. Khan, S. F. Saikh, G. A. T. Sevilla, A. T. Kutbee, R. R. Bahabry, W. Babatain, A. S. Muslem, M. Nour, I. Wicaksono, K. Mishra, in *Proc. IEEE Sensors*, IEEE, Piscataway, NJ **2017**, pp. 1–2.

[20] R. Dahiya, Z. Celik-Butler, L. G. Occhipinti, *IEEE Sens. J.* **2020**, *20*, 7493.

[21] C. T. Chiang, Y. C. Huang, *IEEE Sens. J.* **2006**, *6*, 1564.

[22] A. Kordzadeh, N. De Zanche, *Concepts Magn. Reson., Part B* **2016**, *46*, 19.

[23] S. M. Khan, N. Qaiser, M. M. Hussain, *AIP Adv.* **2019**, *9*, 045118.

[24] V. Leus, D. Elata, *J. Microelectromech. Syst.* **2008**, *17*, 236.

[25] Y. Yang, R. Zhang, L. Zhao, *J. Math. Phys.* **2012**, *53*, 022703.

[26] D. Ha, W. N. De Vries, S. W. M. John, P. P. Irazoqui, W. J. Chappell, *Biomed. Microdevices* **2012**, *14*, 207.

[27] A. S. Nittala, A. Withana, N. Pourjafarian, J. Steimle, in *Proc. of the Conf. on Human Factors in Computing Systems*, Association for Computing Machinery, New York **2018**, pp. 1–12.

[28] G. J. Jeon, H. I. Yeom, T. Jin, J. Kim, J. Yang, S. H. K. Park, *J. Mater. Chem. C* **2020**, *8*, 4271.

[29] L. B. Han, J. N. Ding, S. Wang, J. Xu, N. Y. Yuan, G. G. Cheng, Z. F. Liu, *Sci. China Technol. Sci.* **2018**, *61*, 1137.

[30] J. M. Nassar, K. Mishra, K. Lau, A. A. Aguirre-Pablo, M. M. Hussain, *Adv. Mater. Technol.* **2017**, *2*, 1600228.

[31] M. Jung, S. K. Vishwanath, J. Kim, D. K. Ko, M. J. Park, S. C. Lim, S. Jeon, *Sci. Rep.* **2019**, *9*, 1.

[32] D. J. Lipomi, M. Vosgueritchian, B. C. K. Tee, S. L. Hellstrom, J. A. Lee, C. H. Fox, Z. Bao, *Nat. Nanotechnol.* **2011**, *6*, 788.

[33] J. K. Song, D. Son, J. Kim, Y. J. Yoo, G. J. Lee, L. Wang, M. K. Choi, J. Yang, M. Lee, K. Do, J. H. Koo, N. Lu, J. H. Kim, T. Hyeon, Y. M. Song, D. H. Kim, *Adv. Funct. Mater.* **2017**, *27*, 1605286.

[34] S. Luo, J. Yang, X. Song, X. Zhou, L. Yu, T. Sun, C. Yu, D. Huang, C. Du, D. Wei, *Solid-State Electron.* **2018**, *145*, 29.

[35] A. Ali, A. Khan, K. S. Karimov, A. Ali, A. D. Khan, *J. Nanomater.* **2018**, *2018*, 9592610.

[36] J. Yang, S. Luo, X. Zhou, J. Li, J. Fu, W. Yang, D. Wei, *ACS Appl. Mater. Interfaces* **2019**, *11*, 14997.

[37] X. Shuai, P. Zhu, W. Zeng, Y. Hu, X. Liang, Y. Zhang, R. Sun, C. P. Wong, *ACS Appl. Mater. Interfaces* **2017**, *9*, 26314.

[38] S. Chen, S. Li, S. Peng, Y. Huang, J. Zhao, W. Tang, X. Guo, *J. Semicond.* **2018**, *39*, 013001.

[39] R. B. Mishra, S. F. Shaikh, A. M. Hussain, M. M. Hussain, *AIP Adv.* **2020**, *10*, 055112.

[40] B. U. Hwang, A. Zabeeb, T. Q. Trung, L. Wen, J. D. Lee, Y. I. Choi, H. B. Lee, J. H. Kim, J. G. Han, N. E. Lee, *NPG Asia Mater.* **2019**, *11*, 23.

[41] S. M. Khan, R. B. Mishra, N. Qaiser, A. M. Hussain, M. M. Hussain, *AIP Adv.* **2020**, *10*, 015009.

[42] S. M. Khan, N. Qaiser, S. F. Shaikh, M. M. Hussain, *IEEE Trans. Electron Devices* **2020**, *67*, 249.

[43] J. M. Nassar, M. D. Cordero, A. T. Kutbee, M. A. Karimi, G. A. T. Sevilla, A. M. Hussain, A. Shamim, M. M. Hussain, *Adv. Mater. Technol.* **2016**, *1*, 1600004.

[44] J. M. Nassar, M. M. Hussain, *IEEE Trans. Electron Devices* **2017**, *64*, 2022.

[45] M. Bao, *Analysis and Design Principles of MEMS Devices*, Elsevier, Amsterdam **2005**.

[46] B. Ahmad, R. Pratap, *IEEE Sens. J.* **2011**, *11*, 2426.

[47] L. Lin, H. C. Chu, Y. W. Lu, *J. Microelectromech. Syst.* **1999**, *8*, 514.

[48] L. Lin, W. Yun, in *IEEE Aerospace Conf. Proc. (Vol. 1, Cat. No.98TH8339)*, IEEE, Piscataway, NJ **1998**, pp. 429–436.

[49] R. B. Mishra, S. Santosh Kumar, R. Mukhiya, in *IOP Conf. Series: Materials Science and Engineering*, Vol. *404*, IOP Publishing, Bristol **2018**, p. 012026.

[50] W. P. Eaton, F. Bitsie, J. H. Smith, D. W. Plummer, in *Technical Proc. 1999 Int. Conf. Modeling and Simulation of Microsystems*, San Juan, Puerto Rico **1999**, pp. 640–643.

[51] E. Suhir, *Structural Analysis in Microelectronic and Fiber-Optic Systems: Basic Principles of Engineering Elasticiy and Fundamentals of*

Structural Analysis (Volume-1), Springer Science & Business Media, New York **2012**.

[52] G. Li, D. Li, Y. Cheng, W. Sun, X. Han, C. Wang, *AIP Adv.* **2018**, *8*, 035120.

[53] V. Rochus, B. Wang, H. A. C. Tilmans, A. Ray Chaudhuri, P. Helin, S. Severi, X. Rottenberg, *Mechatronics* **2016**, *40*, 244.

[54] S. P. Timoshenko, S. W. Krieger, *Theory of Plates and Shells*, Tata McGraw-Hill, New Delhi **1959**.

[55] S. Brodetsky, *Nature* **1941**, *148*, 606.

[56] J. N. Reddy, *Theory and Analysis of Elastic Plates and Shells*, CRC Press, Boca Raton, FL **2006**.

[57] M. Molla-Alipour, B. A. Ganji, *Acta Mech. Solida Sin.* **2015**, *28*, 400.

[58] S. E. Navarro, O. Goury, G. Zheng, T. M. Bieze, C. Duriez, *IEEE Robot. Autom. Lett.* **2019**, *4*, 4338.

[59] T. Matsuno, S. Hirai, in *2019 IEEE Int. Conf. Soft Robotics*, IEEE, Piscataway, NJ **2019**, pp. 725–730.

[60] Y. A. Antipov, *Proc. R. Soc. A Math. Phys. Eng. Sci.* **2014**, *470*, 20140064.

[61] W. H. Ko, Q. Wang, *Sens. Actuators, A* **1999**, *75*, 242.

[62] R. B. Mishra, S. R. Nagireddy, S. Bhattacharjee, A. M. Hussain, in *IEEE Conf. Modelling of System Circuits and Devices (MOS-AK India)*, IEEE, Piscataway, NJ **2019**, pp. 17–22.

[63] R. B. Mishra, S. S. Kumar, in *Proc. – IEEE 2nd Int. Conf. on Advances in Computing, Control and Communication Technology*, IEEE, Piscataway, NJ **2018**, pp. 70–74.

[64] D. C. Catling, *Sens. Actuators, A* **1998**, *64*, 157.

[65] R. Prajesh, B. Shankar, N. Jain, A. Agarwal, in *2014 IEEE 2nd Int. Conf. Emerging Electronics*, IEEE, Piscataway, NJ **2014**, pp. 1–3.

[66] H. Liu, J. Zhong, C. Lee, S. W. Lee, L. Lin, *Appl. Phys. Rev.* **2018**, *5*, 041306.

[67] N. Minh-Dung, H. Takahashi, T. Uchiyama, K. Matsumoto, I. Shimoyama, *Appl. Phys. Lett.* **2013**, *103*, 143505.

[68] H. Takahashi, N. M. Dung, K. Matsumoto, I. Shimoyama, *J. Micromech. Microeng.* **2012**, *22*, 055015.

[69] J. Fu, T. Zhu, Y. Liang, Z. Liu, R. Wang, X. Zhang, H. X. Wang, *Sci. Rep.* **2019**, *9*, 4699.

[70] X. Liu, M. Mwangi, X. Li, M. O'Brien, G. M. Whitesides, *Lab Chip* **2011**, *11*, 2189.

[71] M. M. Hamedi, V. E. Campbell, P. Rothemund, F. Güder, D. C. Christodouleas, J. F. Bloch, G. M. Whitesides, *Adv. Funct. Mater.* **2016**, *26*, 2446.

[72] E. J. Maxwell, A. D. Mazzeo, G. M. Whitesides, *MRS Bull.* **2013**, *38*, 309.

[73] A. Fraiwan, H. Lee, S. Choi, *Talanta* **2016**, *158*, 57.

[74] T. K. Kang, *Appl. Phys. Lett.* **2014**, *104*, 073117.

[75] T. Wang, X. Mu, A. B. Randles, Y. Gu, C. Lee, *Appl. Phys. Lett.* **2015**, *107*, 123501.

[76] A. W. Leissa, C. C. Lo, F. W. Niedenfuhr, *AIAA J.* **1965**, *3*, 566.

[77] W. H. Ko, Q. Wang, in *Proc. IEEE Tenth Annual Int. Workshop on Micro Electro Mechanical Systems, An Investigation of Micro Structures Sensors, Actuators, Machines and Robots*, IEEE, Piscataway, NJ **1997**, pp. 284–289.

[78] S. K. Jindal, A. Mahajan, S. K. Raghuwanshi, *Microsyst. Technol.* **2016**, *22*, 1143.

[79] C. Berger, R. Phillips, A. Centeno, A. Zurutuza, A. Vijayaraghavan, *Nanoscale* **2017**, *9*, 17439.

[80] C. Berger, R. Phillips, I. Pasternak, J. Sobieski, W. Strupinski, A. Vijayaraghavan, *2D Mater.* **2018**, *5*, 015025.

[81] R. B. Mishra, S. M. Khan, S. F. Shaikh, A. M. Hussain, M. M. Hussain, in *3rd IEEE Int. Conf. Soft Robotics*, IEEE, Piscataway, NJ **2020**, pp. 194–200.

[82] H. Lv, Q. Guo, G. Hu, in *3rd IEEE Int. Conf. Nano/Micro Engineered and Molecular Systems*, IEEE, Piscataway, NJ **2008**, pp. 796–800.

[83] S. K. Jindal, M. A. Varma, D. Thukral, *Microelectron. J.* **2018**, *73*, 30.

[84] R. B. Mishra, W. Babatain, N. El-Atab, A. M. Hussain, M. M. Hussain, in *15th IEEE Int. Conf. Nano/Micro Engineered and Molecular Systems*, IEEE, Piscataway, NJ **2020**, pp. 95–99.

[85] P. Miao, J. Wang, C. Zhang, M. Sun, S. Cheng, H. Liu, *Nano-Micro Lett.* **2019**, *11*, 71.

[86] Z. He, W. Chen, B. Liang, C. Liu, L. Yang, D. Lu, Z. Mo, H. Zhu, Z. Tang, X. Gui, *ACS Appl. Mater. Interfaces* **2018**, *10*, 12816.

[87] H. Kou, L. Zhang, Q. Tan, G. Liu, H. Dong, W. Zhang, J. Xiong, *Sci. Rep.* **2019**, *9*, 3916.

[88] S. Wan, H. Bi, Y. Zhou, X. Xie, S. Su, K. Yin, L. Sun, *Carbon N. Y.* **2017**, *114*, 209.

[89] K. Ke, M. McMaster, W. Christopherson, K. D. Singer, I. Manas-Zloczower, *Composites, Part A* **2019**, *126*, 105614.

[90] C. Metzger, E. Fleisch, J. Meyer, M. Dansachmüller, I. Graz, M. Kaltenbrunner, C. Keplinger, R. Schwödiauer, S. Bauer, *Appl. Phys. Lett.* **2008**, *92*, 013506.

[91] H. S. Badghaish, M. M. Hussain, *MRS Adv.* **2020**, 1.

[92] O. Atalay, A. Atalay, J. Gafford, C. Walsh, *Adv. Mater. Technol.* **2018**, *3*, 1700237.

[93] C. Parameswaran, D. Gupta, *J. Mater. Chem. C* **2018**, *6*, 5473.

[94] J. Mu, C. Hou, G. Wang, X. Wang, Q. Zhang, Y. Li, H. Wang, M. Zhu, *Adv. Mater.* **2016**, *28*, 9491.

[95] S. J. Park, J. Kim, M. Chu, M. Khine, *Adv. Mater. Technol.* **2016**, *1*, 1600053.

[96] J. Li, L. Fang, B. Sun, X. Li, S. H. Kang, *J. Electrochem. Soc.* **2020**, *167*, 037561.

[97] C. Yang, L. Li, J. Zhao, J. Wang, J. Xie, Y. Cao, M. Xue, C. Lu, *ACS Appl. Mater. Interfaces* **2018**, *10*, 25811.

[98] S. Baek, H. Jang, S. Y. Kim, H. Jeong, S. Han, Y. Jang, D. H. Kim, H. S. Lee, *RSC Adv.* **2017**, *7*, 39420.

[99] Y. Joo, J. Byun, N. Seong, J. Ha, H. Kim, S. Kim, T. Kim, H. Im, D. Kim, Y. Hong, *Nanoscale* **2015**, *7*, 6208.

[100] X. Zeng, Z. Wang, H. Zhang, W. Yang, L. Xiang, Z. Zhao, L. M. Peng, Y. Hu, *ACS Appl. Mater. Interfaces* **2019**, *11*, 21218.

[101] L. Ma, X. Shuai, Y. Hu, X. Liang, P. Zhu, R. Sun, C. P. Wong, *J. Mater. Chem. C* **2018**, *6*, 13232.

[102] J. Cui, B. Zhang, J. Duan, H. Guo, J. Tang, *Sensors (Switzerland)* **2016**, *16*, 2131.

[103] S. R. A. Ruth, V. R. Feig, H. Tran, Z. Bao, *Adv. Funct. Mater.* **2020**, *30*, 2003491.

[104] S. R. A. Ruth, L. Beker, H. Tran, V. R. Feig, N. Matsuhisa, Z. Bao, *Adv. Funct. Mater.* **2020**, *30*, 1903100.

[105] S. C. B. Mannsfeld, B. C. K. Tee, R. M. Stoltenberg, C. V. H. H. Chen, S. Barman, B. V. O. Muir, A. N. Sokolov, C. Reese, Z. Bao, *Nat. Mater.* **2010**, *9*, 859.

[106] B. C. K. Tee, A. Chortos, R. R. Dunn, G. Schwartz, E. Eason, Z. Bao, *Adv. Funct. Mater.* **2014**, *24*, 5427.

[107] M. Li, J. Liang, X. Wang, M. Zhang, *Sensors (Switzerland)* **2020**, *20*, 371.

[108] V. Palaniappan, S. Masihi, M. Panahi, D. Maddipatla, A. K. Bose, X. Zhang, B. B. Narakathu, B. J. Bazuin, M. Z. Atashbar, *IEEE Sens. J.* **2020**, *20*, 7605.

[109] S. H. Cho, S. W. Lee, S. Yu, H. Kim, S. Chang, D. Kang, I. Hwang, H. S. Kang, B. Jeong, E. H. Kim, S. M. Cho, K. L. Kim, H. Lee, W. Shim, C. Park, *ACS Appl. Mater. Interfaces* **2017**, *9*, 10128.

[110] C. M. Boutry, M. Negre, M. Jorda, O. Vardoulis, A. Chortos, O. Khatib, Z. Bao, *Sci. Robot.* **2018**, *3*, eaau6914.

[111] Y. Luo, J. Shao, S. Chen, X. Chen, H. Tian, X. Li, L. Wang, D. Wang, B. Lu, *ACS Appl. Mater. Interfaces* **2019**, *11*, 17796.

[112] N. Bai, L. Wang, Q. Wang, J. Deng, Y. Wang, P. Lu, J. Huang, G. Li, Y. Zhang, J. Yang, K. Xie, X. Zhao, C. F. Guo, *Nat. Commun.* **2020**, *11*, 1.

[113] S. Z. Bisri, S. Shimizu, M. Nakano, Y. Iwasa, *Adv. Mater.* **2017**, *29*, 1607054.

[114] Q. Liu, Z. Liu, C. Li, K. Xie, P. Zhu, B. Shao, J. Zhang, J. Yang, J. Zhang, Q. Wang, C. F. Guo, *Adv. Sci.* **2020**, *7*, 2000348.

[115] B. Nie, S. Xing, J. D. Brandt, T. Pan, *Lab Chip* **2012**, *12*, 1110.

[116] B. Nie, R. Li, J. D. Brandt, T. Pan, *Lab Chip* **2014**, *14*, 1107.

[117] Z. Zhu, R. Li, T. Pan, *Adv. Mater.* **2018**, *30*, 1705122.

[118] Y. Tai, Z. Yang, *Adv. Mater. Interfaces* **2017**, *4*, 1700496.

[119] A. Chhetry, H. Yoon, J. Y. Park, *J. Mater. Chem. C* **2017**, *5*, 10068.

[120] J. Lee, H. Kwon, J. Seo, S. Shin, J. H. Koo, C. Pang, S. Son, J. H. Kim, Y. H. Jang, D. E. Kim, T. Lee, *Adv. Mater.* **2015**, *27*, 2433.

[121] W. Gao, H. Ota, D. Kiriya, K. Takei, A. Javey, *Acc. Chem. Res.* **2019**, *52*, 523.

[122] P. Gould, *Mater. Today* **2003**, *6*, 38.

[123] J. Xiong, J. Chen, P. S. Lee, *Adv. Mater.* **2020**, 2002640.

[124] B. B. Narakathu, A. Eshkeiti, A. S. G. Reddy, M. Rebros, E. Rebrosova, M. K. Joyce, B. J. Bazuin, M. Z. Atashbar, in *Proc. IEEE Sensors*, IEEE, Piscataway, NJ **2012**, pp. 1–4.

[125] A. Eshkeiti, S. Emamian, S. G. R. Avathu, B. B. Narakathu, M. J. Joyce, M. K. Joyce, B. J. Bazuin, M. Z. Atashbar, in *Proc. IEEE Sensors*, IEEE, Piscataway, NJ **2014**, pp. 1192–1195.

[126] S. Khan, L. Lorenzelli, R. S. Dahiya, in *25th Annual SEMI Advanced Semiconductor Manufacturing Conf. (ASMC 2014)*, IEEE, Piscataway, NJ **2014**, p. 219.

[127] D. Maddipatla, B. B. Narakathu, M. M. Ali, A. A. Chlaihawi, M. Z. Atashbar, in *SAS 2017 – IEEE Sensors Applications Symp. Proc.*, IEEE, Piscataway, NJ **2017**, pp. 1–4.

[128] Z. Guo, L. Mo, Y. Ding, Q. Zhang, X. Meng, Z. Wu, Y. Chen, M. Cao, W. Wang, L. Li, *Micromachines* **2019**, *10*, 715.

[129] M. Schouten, R. Sanders, G. Krijnen, in *Proc. IEEE Sensors*, IEEE, Piscataway, NJ **2017**, pp. 1–3.

[130] M. Kisic, N. Blaz, C. Zlebic, L. Zivanov, I. Nikolic, in *40th Int. Spring Seminars on Electronics Technology*, IEEE, Piscataway, NJ **2017**, pp. 1–4.

[131] S. Lee, S. Franklin, F. A. Hassani, T. Yokota, M. O. G. Nayeem, Y. Wang, R. Leib, G. Cheng, D. W. Franklin, T. Someya, *Science* **2020**, *370*, 966.

[132] S. Khan, M. M. Hussain, in *2019 IEEE 16th Int. Conf. Wearable Implant. Body Sens. Networks, BSN 2019*, IEEE, Piscataway, NJ **2019**, pp. 1–4.

[133] G. Mao, X. Huang, M. Diab, J. Liu, S. Qu, *Extreme Mech. Lett.* **2016**, *9*, 139.

[134] H. Godaba, Z. Q. Zhang, U. Gupta, C. Chiang Foo, J. Zhu, *Soft Matter* **2017**, *13*, 2942.

[135] S. R. A. Ruth, V. R. Feig, M. Kim, Y. Khan, J. K. Phong, Z. Bao, *Small Struct.* **2020**, *2*, 2000079.

[136] T. Arbring Sjöström, M. Berggren, E. O. Gabrielsson, P. Janson, D. J. Poxson, M. Seitanidou, D. T. Simon, *Adv. Mater. Technol.* **2018**, *3*, 1700360.

[137] X. Lü, J. Jiang, H. Wang, Q. Gao, S. Zhao, N. Li, J. Yang, S. Wang, W. Bao, R. Chen, *Sensors (Switzerland)* **2019**, *19*, 72.

[138] W. Xiong, D. Guo, Z. Yang, C. Zhu, Y. Huang, *Sci. China Technol. Sci.* **2020**, *63*, 1.

[139] S. W. Janson, H. Helvajian, K. Breuer, in *30th Fluid Dynamics Conf.*, American Institute of Aeronautics and Astronautics, Reston, VA **1999**, p. 3802.

[140] R. Alshanbari, S. Khan, N. El-Atab, M. M. Hussain, in *Proc. IEEE National Aerospace and Electronics Conf.*, IEEE, Piscataway, NJ **2019**, pp. 420–424.

[141] S. Callegari, M. Zagnoni, A. Golfarelli, M. Tartagni, A. Talamelli, P. Proli, A. Rossetti, *Sens. Actuators, A* **2006**, *130–131*, 155.

[142] M. Zagnoni, A. Golfarelli, S. Callegari, A. Talamelli, V. Bonora, E. Sangiorgi, M. Tartagni, *Sens. Actuators, A* **2005**, *123–124*, 240.

[143] H. Shi, M. Al-Rubaiai, C. M. Holbrook, J. Miao, T. Pinto, C. Wang, X. Tan, *Adv. Funct. Mater.* **2019**, *29*, 1809116.

[144] J. Marek, in *Proc. 2011 Int. Symp. VLSI Technology, Systems and Applications*, IEEE, Piscataway, NJ **2011**.

[145] B. P. Gogoi, D. Mladenovic, in *IEEE 28th Annual Conf. on Industrial Electronics Society*, IEEE, Piscataway, NJ **2002**, pp. 2712–2717.

[146] W. J. Fleming, *IEEE Sens. J.* **2001**, *1*, 296.

[147] R. Matsuzaki, A. Todoroki, *Sensors* **2008**, *8*, 8123.

[148] R. Matsuzaki, A. Todoroki, *Sens. Actuators, A* **2007**, *140*, 32.

[149] J. B. Andrews, J. A. Cardenas, C. J. Lim, S. G. Noyce, J. Mullett, A. D. Franklin, *IEEE Sens. J.* **2018**, *18*, 7875.

[150] S. Cruz, D. Dias, J. C. Viana, L. A. Rocha, *IEEE Trans. Instrum. Meas.* **2015**, *64*, 2813.

[151] C. K. Duc, V. P. Hoang, D. T. Nguyen, T. T. Dao, *Polymers (Basel)* **2019**, *11*, 1247.

[152] M. M. Hussain, I. Wicaksono, US20190385097A1, **2019**.

[153] A. Gao, M. Triantafyllou, in *2012 Oceans*, IEEE, Piscataway, NJ **2012**, pp. 1–7.

[154] E. Kanhere, M. Bora, J. Miao, M. Triantafyllou, *Proceedings* **2017**, *1*, 360.

[155] J. M. Nassar, S. M. Khan, S. J. Velling, A. Diaz-Gaxiola, S. F. Shaikh, N. R. Geraldi, G. A. Torres Sevilla, C. M. Duarte, M. M. Hussain, *npj Flexible Electron.* **2018**, *2*, 1.

[156] S. F. Shaikh, H. F. Mazo-Mantilla, N. Qaiser, S. M. Khan, J. M. Nassar, N. R. Geraldi, C. M. Duarte, M. M. Hussain, *Small* **2019**, *15*, 1804385.

[157] A. S. Almuslem, S. F. Shaikh, M. M. Hussain, *Adv. Mater. Technol.* **2019**, *4*, 1900145.

[158] S. F. Shaikh, M. M. Hussain, *Appl. Phys. Lett.* **2020**, *117*, 074101.

[159] D. M. Vogt, Y. Menguc, Y.-L. Park, M. F. Wehner, R. Kramer, C. Majidi, L. P. Jentoft, Y. Tenzer, R. Howe, R. J. Wood, in *Proc. of the Int. Workshop on Research Frontiers in Electronics Skin Technology*, IEEE, Piscataway, NJ **2013**, pp. 1–2.

[160] Z. Zhan, R. Lin, V. T. Tran, J. An, Y. Wei, H. Du, T. Tran, W. Lu, *ACS Appl. Mater. Interfaces* **2017**, *9*, 37921.

[161] B. C. K. Tee, C. Wang, R. Allen, Z. Bao, *Nat. Nanotechnol.* **2012**, *7*, 825.

[162] L. Chin, M. C. Yuen, J. Lipton, L. H. Trueba, R. Kramer-Bottiglio, D. Rus, in *Proc. – IEEE Int. Conf. Robotics Automation*, IEEE, Piscataway, NJ **2019**, pp. 2765–2771.

[163] L. Chin, J. Lipton, M. C. Yuen, R. Kramer-Bottiglio, D. Rus, in *2nd IEEE Int. Conf. Soft Robotics*, IEEE, Piscataway, NJ **2019**, pp. 102–107.

[164] J. Hashizume, T. M. Huh, S. A. Suresh, M. R. Cutkosky, *IEEE Robot. Autom. Lett.* **2019**, *4*, 677.

[165] T. M. Huh, H. Choi, S. Willcox, S. Moon, M. R. Cutkosky, *IEEE Robot. Autom. Lett.* **2020**, *5*, 2562.

[166] M. Amit, R. K. Mishra, Q. Hoang, A. M. Galan, J. Wang, T. N. Ng, *Mater. Horiz.* **2019**, *6*, 604.

[167] W. Navaraj, R. Dahiya, *Adv. Intell. Syst.* **2019**, *1*, 1900051.

[168] R. P. Rocha, P. A. Lopes, A. T. De Almeida, M. Tavakoli, C. Majidi, *J. Micromech. Microeng.* **2018**, *28*, 034001.

[169] M. Ntagios, H. Nassar, A. Pullanchiyodan, W. T. Navaraj, R. Dahiya, *Adv. Intell. Syst.* **2020**, *2*, 1900080.

[170] Z. Ji, H. Zhu, H. Liu, T. Chen, L. Sun, in *2016 International Conference on Advanced Robotics and Mechatronics*, IEEE, Piscataway, NJ, **2016**, pp. 207–212.

[171] P. Roberts, D. D. Damian, W. Shan, T. Lu, C. Majidi, in *IEEE Int. Conf. Robotics and Automation*, IEEE, Piscataway, NJ **2013**, pp. 3525–3534.

[172] P. Maiolino, M. Maggiali, G. Cannata, G. Metta, L. Natale, *IEEE Sens. J.* **2013**, *13*, 3910.

[173] R. Ramalingame, A. Lakshmanan, F. Müller, U. Thomas, O. Kanoun, *J. Sens. Sens. Syst.* **2019**, *8*, 87.

[174] S. Wang, K. H. Huang, Y. J. Yang, in *20th Int. Conf. Solid-State Sensors, Actuators Microsystems Eurosensors XXXIII (TRANSDUCERS EUROSENSORS XXXIII)*, IEEE, Piscataway, NJ **2019**, pp. 458–461.

**ADVANCED
SCIENCE NEWS**

www.advancedsciencenews.com

**ADVANCED
MATERIALS
TECHNOLOGIES**

www.advmattechnol.de

[175] A. Gruebele, J. P. Roberge, A. Zerbe, W. Ruotolo, T. M. Huh, M. R. Cutkosky, *IEEE Robot. Autom. Lett.* **2020**, *5*, 1750.

[176] H. A. Sonar, M. C. Yuen, R. Kramer-Bottiglio, J. Paik, in *IEEE Int. Conf. Soft Robotics*, IEEE, Piscataway, NJ **2018**, pp. 170–175.

[177] L. DeFrancesco, I. Jarchum, *Nat. Biotechnol.* **2019**, *37*, 329.

[178] T. Someya, M. Amagai, *Nat. Biotechnol.* **2019**, *37*, 382.

[179] M. A. McEvoy, N. Correll, *Science* **2015**, *347*, 1261689.

[180] E. Waltz, *Nat. Biotechnol.* **2019**, *37*, 340.

[181] W. Gao, S. Emaminejad, H. Y. Y. Nyein, S. Challa, K. Chen, A. Peck, H. M. Fahad, H. Ota, H. Shiraki, D. Kiriya, D.-H. Lien, G. A. Brooks, R. W. Davis, A. Javey, *Nature* **2016**, *529*, 509.

[182] Y. Khan, A. E. Ostfeld, C. M. Lochner, A. Pierre, A. C. Arias, *Adv. Mater.* **2016**, *28*, 4373.

[183] J. Heikenfeld, A. Jajack, J. Rogers, P. Gutruf, L. Tian, T. Pan, R. Li, M. Khine, J. Kim, J. Wang, J. Kim, *Lab Chip* **2018**, *18*, 217.

[184] Kenry, J. C. Yeo, C. T. Lim, *Microsyst. Nanoeng.* **2016**, *2*, 16043.

[185] S. Lee, Q. Shi, C. Lee, *APL Mater.* **2019**, *7*, 031302.

[186] N. El-Atab, R. B. Mishra, F. Al-Modaf, L. Joharji, A. A. Alsharif, H. Alamoudi, M. Diaz, N. Qaiser, M. M. Hussain, *Adv. Intell. Syst.* **2020**, *2*, 2000128.

[187] Y. Zang, F. Zhang, C. A. Di, D. Zhu, *Mater. Horiz.* **2015**, *2*, 140.

[188] L. Ma, X. Yu, Y. Yang, Y. Hu, X. Zhang, H. Li, X. Ouyang, P. Zhu, R. Sun, C. ping Wong, *J. Materiomics* **2020**, *6*, 321.

[189] A. M. Hussain, E. B. Lizardo, G. A. Torres Sevilla, J. M. Nassar, M. M. Hussain, *Adv. Healthcare Mater.* **2015**, *4*, 665.

[190] R. Shi, Z. Lou, S. Chen, G. Shen, *Sci. China Mater.* **2018**, *61*, 1587.

[191] X. Zhao, Z. Zhang, Q. Liao, X. Xun, F. Gao, L. Xu, Z. Kang, Y. Zhang, *Sci. Adv.* **2020**, *6*, eaba4294.

[192] B. W. An, S. Heo, S. Ji, F. Bien, J. U. Park, *Nat. Commun.* **2018**, *9*, 1.

[193] H.-K. Kim, S. Lee, K.-S. Yun, *Sens. Actuators, A* **2011**, *165*, 2.

[194] J. Li, Z. Ma, H. Wang, X. Gao, Z. Zhou, R. Tao, L. Pan, Y. Shi, *Adv. Intell. Syst.* **2019**, *1*, 1900063.

[195] J. C. Yang, J. O. Kim, J. Oh, S. Y. Kwon, J. Y. Sim, D. W. Kim, H. B. Choi, S. Park, *ACS Appl. Mater. Interfaces* **2019**, *11*, 19472.

[196] Y. Yu, J. Nassar, C. Xu, J. Min, Y. Yang, A. Dai, R. Doshi, A. Huang, Y. Song, R. Gehlhar, A. D. Ames, W. Gao, *Sci. Robot.* **2020**, *5*, eaaz7946.

[197] M. Kaisti, T. Panula, J. Leppänen, R. Punkkinen, M. Jafari Tadi, T. Vasankari, S. Jaakkola, T. Kiviniemi, J. Airaksinen, P. Kostiainen, U. Meriheinä, T. Koivisto, M. Pänkäälä, *npj Digital Med.* **2019**, *2*, 39.

[198] Z. Lou, S. Chen, L. Wang, K. Jiang, G. Shen, *Nano Energy* **2016**, *23*, 7.

[199] L. Y. Chen, B. C. K. Tee, A. L. Chortos, G. Schwartz, V. Tse, D. J. Lipomi, H. S. P. Wong, M. V. McConnell, Z. Bao, *Nat. Commun.* **2014**, *5*, 1.

[200] K. H. Huang, F. Tan, T. D. Wang, Y. J. Yang, *Sensors (Switzerland)* **2019**, *19*, 848.

[201] K. Meng, J. Chen, X. Li, Y. Wu, W. Fan, Z. Zhou, Q. He, X. Wang, X. Fan, Y. Zhang, J. Yang, Z. L. Wang, *Adv. Funct. Mater.* **2019**, *29*, 1806388.

[202] C. L. Choong, M. B. Shim, B. S. Lee, S. Jeon, D. S. Ko, T. H. Kang, J. Bae, S. H. Lee, K. E. Byun, J. Im, Y. J. Jeong, C. E. Park, J. J. Park, U. I. Chung, *Adv. Mater.* **2014**, *26*, 3451.

[203] T. Someya, T. Sekitani, S. Iba, Y. Kato, H. Kawaguchi, T. Sakurai, *Proc. Natl. Acad. Sci. USA* **2004**, *101*, 9966.

[204] G. Schwartz, B. C. K. Tee, J. Mei, A. L. Appleton, D. H. Kim, H. Wang, Z. Bao, *Nat. Commun.* **2013**, *4*, 1859.

[205] X. Yang, Z.-M. Cao, Y. Chen, D. Wu, X.-B. Qiu, D. Yu, X.-L. Guo, *Extreme Mech. Lett.* **2020**, *37*, 100715.

[206] C. Wang, X. Li, H. Hu, L. Zhang, Z. Huang, M. Lin, Z. Zhang, Z. Yin, B. Huang, H. Gong, S. Bhaskaran, Y. Gu, M. Makihata, Y. Guo, Y. Lei, Y. Chen, C. Wang, Y. Li, T. Zhang, Z. Chen, A. P. Pisano, L. Zhang, Q. Zhou, S. Xu, *Nat. Biomed. Eng.* **2018**, *2*, 687.

[207] B. Zhuo, S. Chen, M. Zhao, X. Guo, *IEEE J. Electron Devices Soc.* **2017**, *5*, 219.

[208] M. Singla, S. Azeemuddin, P. Sistla, *IEEE J. Transl. Eng. Health Med.* **2020**, *8*, 1.

[209] J. S. Williams, S. M. Brown, P. R. Conlin, *N. Engl. J. Med.* **2009**, *360*, e6.

[210] C. K. W. Lai, R. Beasley, J. Crane, S. Foliaki, J. Shah, S. Weiland, N. Aït-Khaled, H. R. Anderson, M. I. Asher, R. Beasley, B. Björksten, B. Brunekreef, J. Crane, P. Ellwood, C. Flohr, S. Foliaki, F. Forastiere, L. García-Marcos, U. Keil, C. K. W. Lai, J. Mallol, E. A. Mitchell, S. Montefort, J. Odhiambo, N. Pearce, C. F. Robertson, J. Shah, A. W. Stewart, D. Strachan, E. von Mutius, et al., *Thorax* **2009**, *64*, 476.

[211] W. W. Flemons, M. R. Littner, J. A. Rowley, P. Gay, W. M. Anderson, D. W. Hudgel, R. D. McEvoy, D. I. Loube, *Chest* **2003**, *124*, 1543.

[212] S. Sharma, A. Chhetry, M. Sharifuzzaman, H. Yoon, J. Y. Park, *ACS Appl. Mater. Interfaces* **2020**, *12*, 22212.

[213] S. W. Park, P. S. Das, A. Chhetry, J. Y. Park, *IEEE Sens. J.* **2017**, *17*, 6558.

[214] S. S. Zulkifli, W. P. Loh, *Foot Ankle Surg.* **2020**, *26*, 25.

[215] M. J. Rupérez, J. D. Martín-Guerrero, C. Monserrat, M. Alcañiz, *Expert Syst. Appl.* **2012**, *39*, 5349.

[216] S. Qiu, L. Liu, H. Zhao, Z. Wang, Y. Jiang, *Micromachines* **2018**, *9*, 442.

[217] C. S. Morère, Ł. Surazyński, A. R. Pérez-Tabernero, E. Vihriälä, T. Myllylä, *J. Sens.* **2016**, *2016*, 1.

[218] M. F. Domingues, N. Alberto, C. S. J. Leitao, C. Tavares, E. R. De Lima, A. Radwan, V. Sucasas, J. Rodriguez, P. S. B. Andre, P. F. C. Antunes, *IEEE Internet Things J.* **2019**, *6*, 207.

[219] Y. Xia, Y. Li, L. Xun, Q. Yan, D. Zhang, *Gait Posture* **2019**, *68*, 403.

[220] F. Horst, S. Lapuschkin, W. Samek, K. R. Müller, W. I. Schöllhorn, *Sci. Rep.* **2019**, *9*, 2391.

[221] K. F. Lei, K. F. Lee, M. Y. Lee, *Microelectron. Eng.* **2012**, *99*, 1.

[222] S. W. Park, P. S. Das, J. Y. Park, *Org. Electron.* **2018**, *53*, 213.

[223] J. Tao, M. Dong, L. Li, C. Wang, J. Li, Y. Liu, R. Bao, C. Pan, *Microsyst. Nanoeng.* **2020**, *6*, 1.

[224] L. M. Abraham, N. C. R. Epasinghe, D. Selva, R. Casson, *Eye* **2008**, *22*, 503.

[225] K. R. Ficarrotta, Y. H. Mohamed, C. L. Passaglia, *Sci. Rep.* **2020**, *10*, 126.

[226] J. C. Hamzah, Q. Daka, A. Azuara-Blanco, *Eye* **2020**, *34*, 155.

[227] P. J. Chen, D. C. Rodger, R. Agrawal, S. Saati, E. Meng, R. Varma, M. S. Humayun, Y. C. Tai, *J. Micromech. Microeng.* **2007**, *17*, 1931.

[228] S. Lizón-Martínez, R. Giannetti, J. L. Rodríguez-Marrero, B. Tellini, *IEEE Trans. Instrum. Meas.* **2005**, *54*, 1534.

[229] J. Coosemans, M. Catrysse, R. Puers, *Sens. Actuators, A* **2004**, *110*, 432.

[230] R. N. Rizq, W. H. Choi, D. Eilers, M. M. Wright, B. Ziaie, *Br. J. Ophthalmol.* **2001**, *85*, 868.

[231] S. Aravamudhan, in *MEMS Biomed. Appl.* **2012**, pp. 81.

[232] Y. Chiu, Y. Z. Chen, C. C. Hsieh, H. C. Hong, in *Proc. IEEE Sensors*, IEEE, Piscataway, NJ **2019**, pp. 1–4.

[233] M. M. Ghanbari, J. M. Tsai, A. Nirmalathas, R. Muller, S. Gambini, *IEEE J. Solid-State Circuits* **2017**, *52*, 720.

[234] M. H. Behfar, T. Björninen, E. Moradi, L. Sydänheimo, L. Ukkonen, *Int. J. Antennas Propag.* **2015**, *2015*, 1.

[235] Q. Wei, C. He, J. Chen, D. Chen, J. Wang, *IEEE Trans. Electron Devices* **2018**, *19*, 721.

[236] K. Lee, J. Lee, G. Kim, Y. Kim, S. Kang, S. Cho, S. G. Kim, J. K. Kim, W. Lee, D. E. Kim, S. Kang, D. E. Kim, T. Lee, W. Shim, *Small* **2017**, *13*, 1700368.

[237] S. Takamatsu, T. Lonjaret, E. Ismailova, A. Masuda, T. Itoh, G. G. Malliaras, *Adv. Mater.* **2016**, *28*, 4485.

[238] X. Wang, T. Xu, S. Dong, S. Li, L. Yu, W. Guo, H. Jin, J. Luo, Z. Wu, J. M. King, *RSC Adv.* **2017**, *7*, 48461.

[239] X. Liang, H. Heidari, R. Dahiya, in *Proc. 1st New Generation of Circuits and Systems Conf.*, IEEE, Piscataway, NJ **2017**, pp. 181–184.

[240] X. Liang, R. Ghannam, H. Heidari, *IEEE Sens. J.* **2019**, *19*, 1082.

[241] S. Masihi, M. Z. Atashbar, M. Panahi, D. Maddipatla, A. K. Bose, X. Zhang, A. J. Hanson, V. Palaniappan, B. B. Narakathu, B. J. Bazuin, in *Proc. IEEE Sensors*, IEEE, Piscataway, NJ **2019**, pp. 1–4.

[242] X. Wang, T. Li, J. Adams, J. Yang, *J. Mater. Chem. A* **2013**, *1*, 3580.

[243] J. A. Dobrzynska, M. A. M. Gijs, *J. Micromech. Microeng.* **2013**, *23*, 015009.

[244] K. F. Lei, K. F. Lee, M. Y. Lee, *Microsyst. Technol.* **2014**, *20*, 1351.

[245] S. Yao, Y. Zhu, *Nanoscale* **2014**, *6*, 2345.

[246] B. Zhang, Z. Xiang, S. Zhu, Q. Hu, Y. Cao, J. Zhong, Q. Zhong, B. Wang, Y. Fang, B. Hu, J. Zhou, Z. Wang, *Nano Res.* **2014**, *7*, 1488.

[247] J. Wang, J. Jiu, M. Nogi, T. Sugahara, S. Nagao, H. Koga, P. He, K. Suganuma, *Nanoscale* **2015**, *7*, 2926.

[248] B. Y. Lee, J. Kim, H. Kim, C. Kim, S. D. Lee, *Sens. Actuators, A* **2016**, *240*, 103.

[249] C. Mu, J. Li, Y. Song, W. Huang, A. Ran, K. Deng, J. Huang, W. Xie, R. Sun, H. Zhang, *ACS Appl. Nano Mater.* **2018**, *1*, 274.

[250] H. Kim, G. Kim, T. Kim, S. Lee, D. Kang, M. S. Hwang, Y. Chae, S. Kang, H. Lee, H. G. Park, W. Shim, *Small* **2018**, *14*, 1703432.

[251] Q. Zhang, W. Jia, C. Ji, Z. Pei, Z. Jing, Y. Cheng, W. Zhang, K. Zhuo, J. Ji, Z. Yuan, S. Sang, *Smart Mater. Struct.* **2019**, *28*, 115040.

[252] X. Yang, Y. Wang, H. Sun, X. Qing, *Sens. Actuators, A* **2019**, *285*, 67.

[253] Bijender, A. Kumar, Bijendar, A. Kumar, *ACS Omega* **2020**, *5*, 16944.

[254] M. Pruvost, W. J. Smit, C. Monteux, P. Poulin, A. Colin, *npj Flexible Electron.* **2019**, *3*, 7.

[255] Y. Jung, W. Lee, K. Jung, B. Park, J. Park, J. Ko, H. Cho, *Polymers (Basel)* **2020**, *12*, 1412.

[256] Y. Xiong, Y. Shen, L. Tian, Y. Hu, P. Zhu, R. Sun, C. P. Wong, *Nano Energy* **2020**, *70*, 104436.

[257] G. Y. Bae, J. T. Han, G. Lee, S. Lee, S. W. Kim, S. Park, J. Kwon, S. Jung, K. Cho, *Adv. Mater.* **2018**, *30*, 1803388.

[258] W. Cheng, J. Wang, Z. Ma, K. Yan, Y. Wang, H. Wang, S. Li, Y. Li, L. Pan, Y. Shi, *IEEE Electron Device Lett.* **2018**, *39*, 288.

[259] E. Thouti, A. Nagaraju, A. Chandran, P. V. B. S. Prakash, P. Shivanarayanamurthy, B. Lal, P. Kumar, P. Kothari, D. Panwar, *Sens. Actuators, A* **2020**, *314*, 112251.

[260] T. Shao, J. Wu, Y. Zhang, Y. Cheng, Z. Zuo, H. Lv, M. Ying, C. P. Wong, Z. Li, *Adv. Mater. Technol.* **2020**, *5*, 2000032.

[261] J. Wu, Y. Yao, Y. Zhang, T. Shao, H. Wu, S. Liu, Z. Li, L. Wu, *Nanoscale* **2020**, *12*, 21198.

[262] E. G. Bakhoum, M. H. M. Cheng, *J. Microelectromech. Syst.* **2010**, *19*, 443.

Rishabh B. Mishra is currently pursuing his M.S. degree in Electronics and Communication Engineering from International Institute of Information Technology (IIIT), Hyderabad. He worked as a full time research trainee at CSIR-Central Electronics Engineering Research Institute (CEERI) from July-2017 to June-2020 and summer research trainee at CSIR-National Aerospace Laboratories (NAL), Bangalore during June to August, 2020. Currently, he is a visiting student in Electrical and Computer Engineering, King Abdullah University of Science and Technology (KAUST), Saudi Arabia, under the guidance of Prof. Muhammad M. Hussain. His research interests are flexible and stretchable electronics, low-cost MEMS devices, soft robotics, and sensing/actuation.

Nazek El-Atab received her Ph.D. degree in Interdisciplinary Engineering from the Masdar Institute of Science and Technology under a cooperative program with the MIT, in 2017, funded by the Office of Naval Research Global. She is currently a research scientist with Prof. Muhammad Mustafa Hussain at the MMH labs at King Abdullah University of Science and Technology (KAUST), Saudi Arabia. Her current research focuses on the design and fabrication of futuristic electronics. She is also currently serving as associate editor of Nano Select (Wiley) and review editor of Flexible Electronics (Frontiers in Electronics).

Aftab M. Hussain is currently an assistant professor at International Institute of Information Technology (IIIT) Hyderabad and the Principal Investigator of the PATRIoT Lab. He earned his Bachelor's degree from IIT Roorkee, M.S. and Ph.D. from KAUST, followed by postdoctoral fellowship at Harvard University. He has more than nine years of experience working with device fabrication, thin film characterization and device testing, along with sensor applications in IoT and related areas. He is a member of the Executive Committee (ExeCom) of IEEE CAS/EDS joint chapter in Hyderabad.

Muhammad Hussain is a professor of EECS, University of California Berkeley. His research is focused on futuristic electronics. He is a fellow of IEEE, American Physical Society, and Institute of Physics (UK), and a distinguished lecturer of IEEE Electron Devices Society, and an editor of IEEE T-ED.